Evaluation of Single Crystal LaB_6 Cathodes for Use in a High Frequency Backward Wave Oscillator Tube

Interim Report

For the Period

July 1, 1983 to January 1, 1984

by

L. W. Swanson

P. R. Davis

G. A. Schwind

Oregon Graduate Center

19600 N.W. Walker Road

Beaverton, Oregon 97006

Supported by NASA Grant NAG3-434

From The

NASA-Lewis Research Center

Cleveland, Ohio

TABLE OF CONTENTS

Abstract

In this progress report the results of thermionic emission and evaporation studies of single crystal LaB_6 cathodes are given. A comparison between the (100), (210) and (310) crystal planes shows the (310) and (210) planes to possess a work function ~ 0.2 eV lower than (100). This translates into a significant increase in current density, J, at a specified temperature. Comparison with a state-of-the-art impregnated dispenser cathode shows that LaB_6(310) is a superior cathode in nearly all respects except operating temperature at $J < 10$ A/cm^2. The 1600 K thermionic and room temperature retarding potential work functions for LaB_6(310) are 2.42 and 2.50 respectively.

I. Introduction

In this report we summarize the progress made during the first 7 months of the LaB_6 cathode study being carried out by OGC. The primary objective of this study is to determine the best performing LaB_6 crystal face for a flat cathode thermionic emitter. It is expected that this evaluation will include measurement of the emitted current density/temperature relationships and cathode evaporation rates. In addition, the effect of ambient gas pressure on cathode performance will be evaluated.

The ultimate purpose of this investigation is to provide a well characterized, high current density (e.g. 10 to 30 A/cm^2) cathode for a high frequency backward wave oscillator (BWO) traveling wave tube (TWT). Such a tube is expected to have applications in space instrumentation involving microwave spectroscopy. In addition to cathode evaluation, several cathode structures will be fabricated and delivered to the University of Utah for evaluation in a gun structure being developed for the BWO TWT.

In Appendix I is a paper to be submitted to Surface Science involving some of the results of this program along with previous results.

II. Experimental Approach

1. Single Crystal Preparation

Single crystals of high purity LaB_6 and CeB_6 were prepared by a zone melting technique described elsewhere.[1] Single crystal rods up to several cm length and 1 to 3mm in diameter can be prepared by this technique. In addition, a particular crystallographic direction can be made to fall along the rod axis by using a "seed" crystal with the desired orientation.

A centerless grinder was used to bring the single crystal rod diameter down to a specified value (not less than 0.5mm). Small lengths of the single crystal rod were sliced off using a diamond saw. After polishing one of the crystal faces to a mirror finish, using a diamond grinding wheel and diamond paste polish, the crystal was checked by a Laue x-ray camera to accurately determine the crystallographic direction perpendicular to the polished surface.

In previous work[2] it was determined that the stoichiometry of the rare earth hexaborides dramatically affected the work function and evaporation rate. Thus, the stoichometry of the starting material was carefully controlled in order to provide a known final stoichiometry after zone melting. Typically for LaB_6 the stoichiometry of the starting material was B/La = 6.2 which resulted in a final value of B/La = 6.09 after zone melting. For CeB_6 crystals the final stoichiometry was B/Ce = 6.2.

2. Cathode Mounting

Mounting rare earth hexaboride specimens in suitable containers for subsequent heating has historically been a difficult task due to the rapid interaction of the RB_6 with most refractory materials at elevated temperature. The general consensus of the literature on this subject is that C, Re and Ta are the only suitable mounting materials for LaB_6 at T $\simeq$ 1900 K. Typically B diffuses into the mounting material causing the adjacent LaB_6 to convert to the lower melting point compound LaB_4.

In this study a Re cup mount developed by FEI Company, Hillsboro, Oregon, was used to mount the RB_6 crystals. Such a mounting structure, as shown in Figure 1 has proven to be durable for several hundred hours of cathode operation at 1800 to 1900 K. As shown in Figure 1 a .13 mm diameter wire for resistive heating is spot welded to a 0.84 mm diameter Re cup. A .77 mm

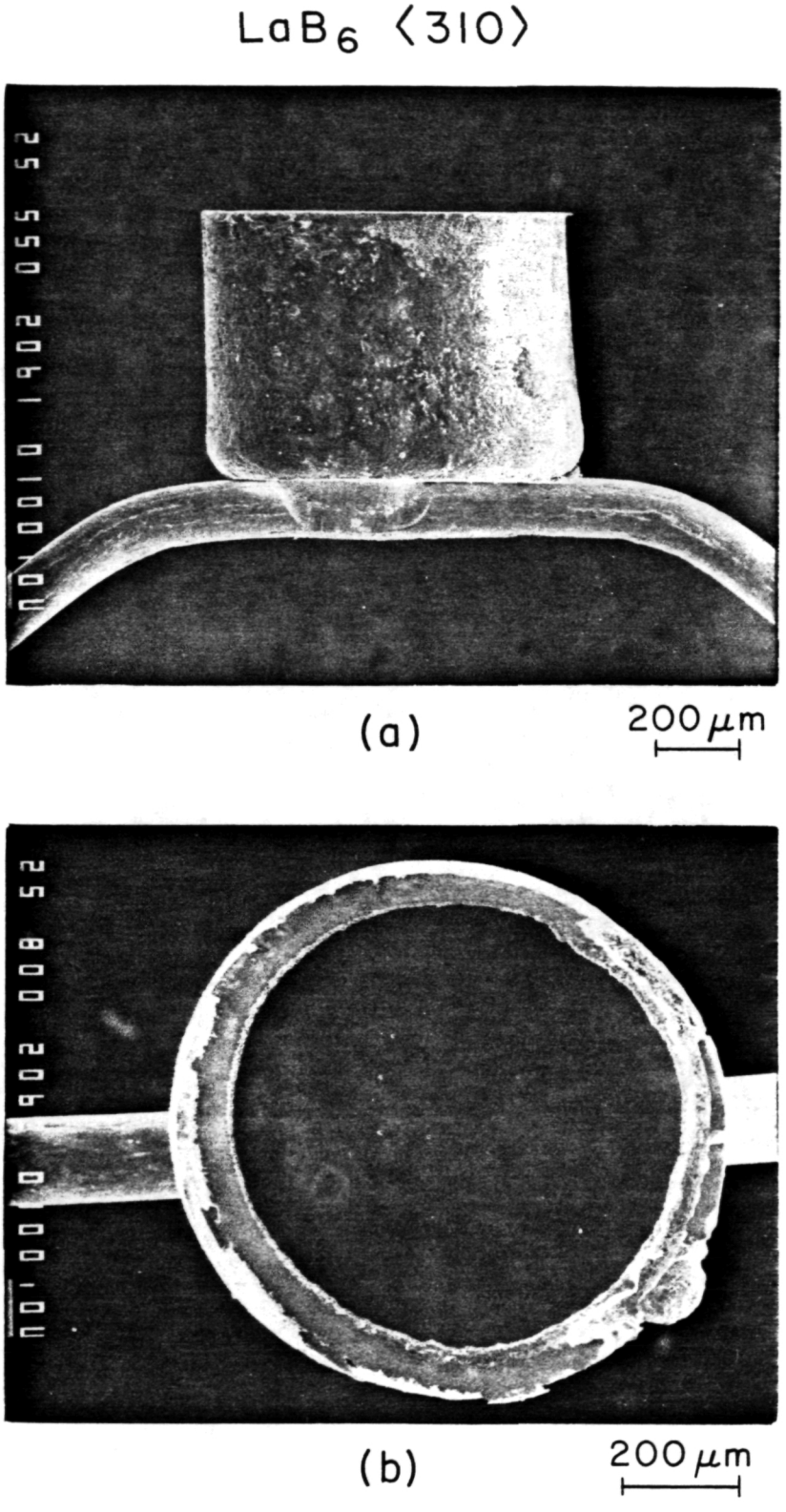

Figure 1. SEM photos of a directly heated LaB_6 flat cathode mounted in a Re cup.

diameter crystal is inserted into the Re cup as shown in Figure 1 for a flat crystal or as shown in Figure 2 for a conically shaped LaB_6 crystal. By use of a faceter wheel various shaped crystals can be fabricated.

3. Vaporization Measurements

The evaporation rate of the single crystal surfaces was determined by carefully measuring the thickness of material removed by heating the crystal for a known time at a specified temperature. The dimensional changes of the crystals were measured by comparison of SEM photographs taken before and after the heating. Evaporation measurements were carried out in an ultra-high vacuum chamber with a leak valve through which a partial pressure of O_2 could be maintained during the evaporation.

Temperature was monitored with a micropyrometer with appropriate correction for the emissivity of the LaB_6.[3] Heating power requirements for the Figures 1 and 2 type cathode structures are given in Figure 3. Typically, the cathode heating power at 1800K is 2.5 W. Since the primary heat loss is through radiation a smaller cathode diameter will result in a lower heater power requirement.

4. Work Function Measurements

Work functions of the cathodes were measured by two methods. A room temperature measurement was made using a field emission retarding potential (FERP) technique. This method, which is described in detail elsewhere,[4] is unique in that the absolute work function of the target material is measured.

The other method of work function measurement used a planar thermionic diode, with application of the well known Richardson-Dushman equation where the emitter current density J, work function ϕ_e and applied field F are related as follows:

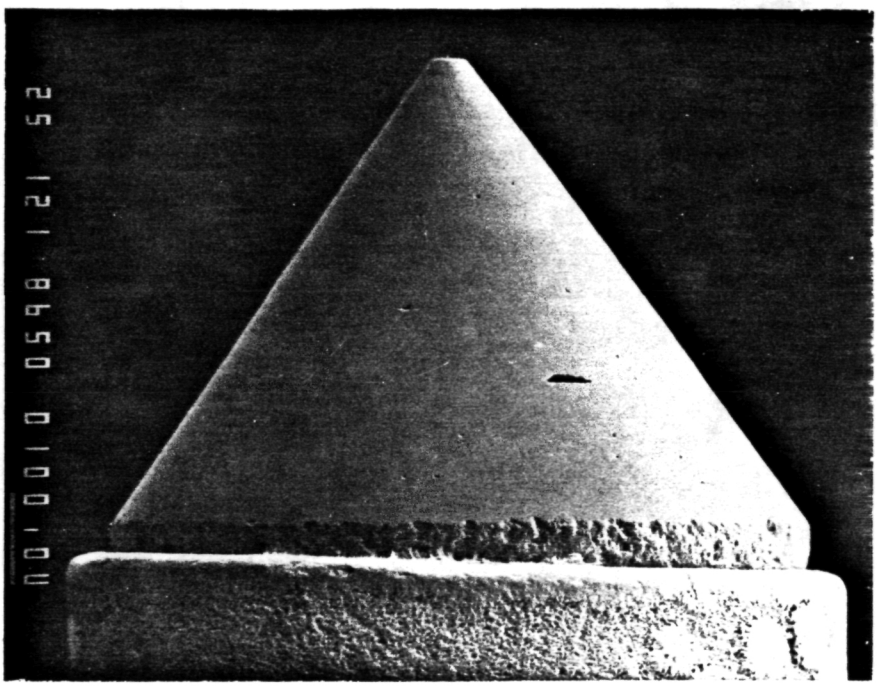

Figure 2. SEM photo of a truncated, 70° cone full angle, <100> oriented LaB_6 emitter before life test.

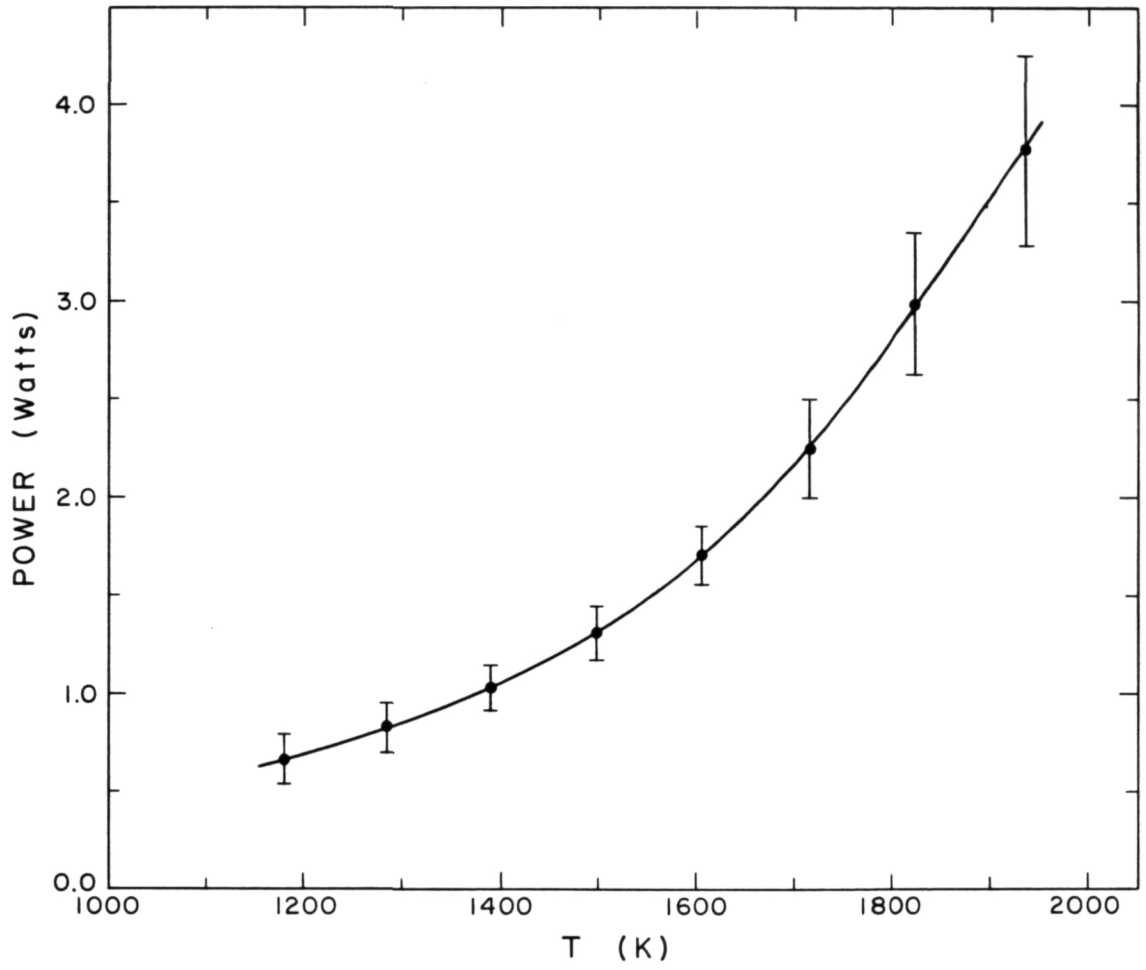

Figure 3. Graph shows heating power vs emitter temperature for Figure 1 type cathode structure.

$$\phi_e(T,F) = -kT \ln(J/120T^2) \quad (1)$$

and

$$\phi_e(T,F) = \phi_e(T) - 3.8F^{1/2} \quad (2)$$

In the above equations the units are as follows: ϕ_e(eV), F(V/Å) and J(A/cm^2). Using Eq.(1) the value of ϕ_e is determined experimentally as a function of F at various values of T. Then, applying Eq.(2), a Schottky plot of $\phi_e(T)$ vs $F^{1/2}$ is made at each value of T and the zero field value $\phi_o(T)$ is determined. In this way the temperature dependence of ϕ_o can be explicitly shown. Note that for a planar diode geometry, the field F is given by V/d, where V is the applied voltage and d is the diode spacing in cm.

III. Results

1. Evaporation Studies

The evaporation rates have been measured for various cathode shapes in low background pressure (~ 1 x 10^{-8} torr) and in the presence of various pressures of oxygen gas. From previous studies[5] it is known that partial pressures of O_2 can greatly enhance the evaporation rate of LaB_6 by formation of volatile oxides of La and B. Because of their oxidizing capabilities it is expected that O_2, H_2O and perhaps CO_2 are the most likely gases to significantly enhance the evaporation rates.

a) Low Pressure Results

With only the background gases common to an unbaked high vacuum system, where typically P ~ 2 x 10^{-8} torr, the evaporation rate vs temperature was measured for $LaB_{6.09}$ as depicted in curve (a) of Figure 4. The mass loss rate (R_m) and thickness loss rate (R_T), for evaporation with $P \lesssim 2 \times 10^{-8}$ torr, are given by

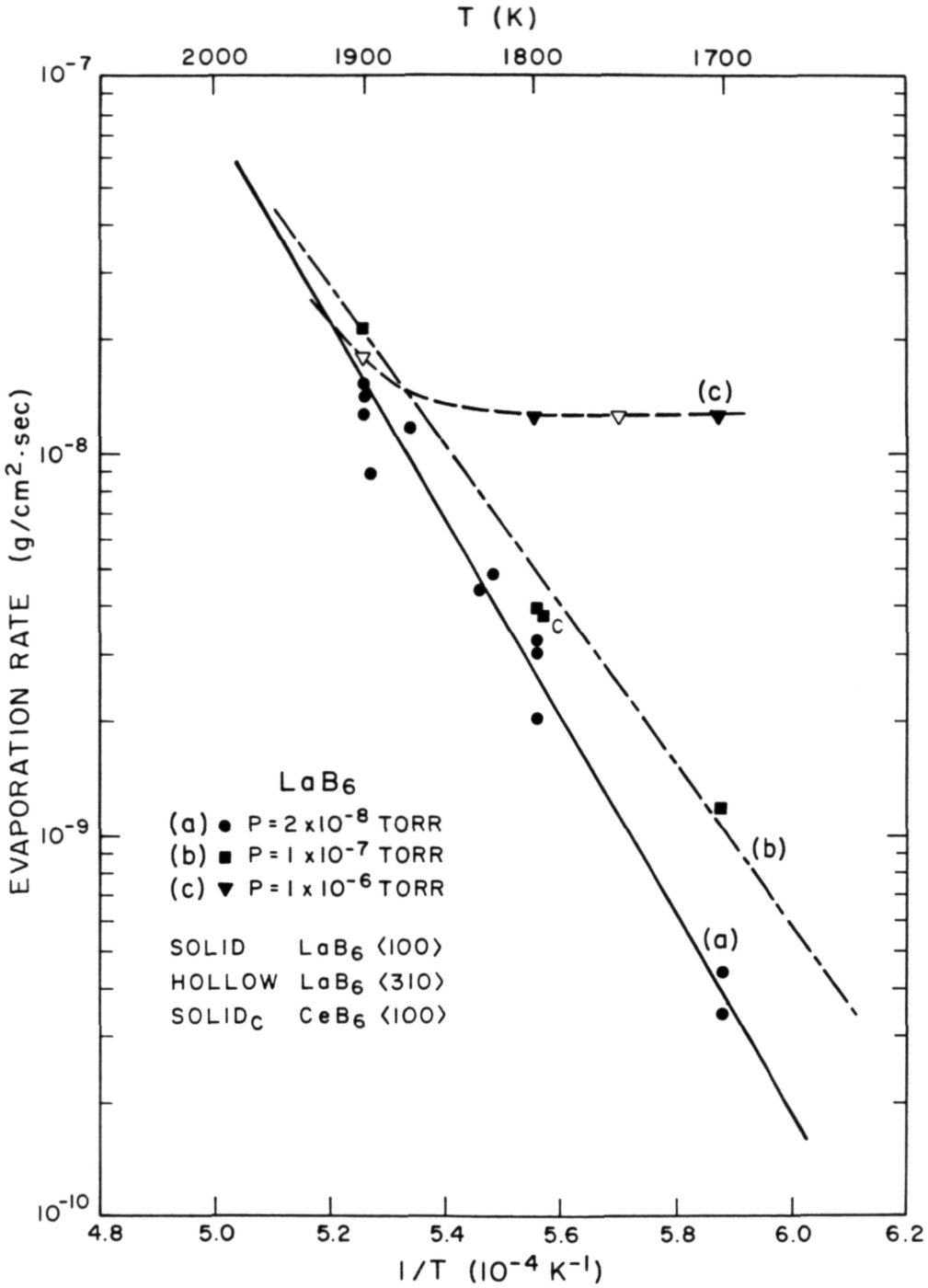

Figure 4. Evaporation rate vs emitter temperature for the indicated emitter orientation and oxygen pressure. Evaporation rates were measured by change in diameter of the cylindrical portion of the emitter.

$$R_m = 1.13 \times 10^6 \exp(-60524/T) \ (g/cm^2\text{-sec}) \quad (3)$$

$$R_T = 7.57 \times 10^{16} \exp(-60524/T) \ (\mu m/yr) \quad (4)$$

In obtaining curve (a) the change in diameter of a <100> oriented $LaB_{6.09}$ crystal was measured using the cathode shape of Figure 2. By using a conical structure with either a 70 or 90° cone angle we are able to ascertain whether evaporation occurs isotropically or whether it varies with crystal face. As shown in Figure 5(a), the cross section of the conical shaped portion of a pointed, conically shaped emitter remains circular after evaporation of 62 μm of material. Thus we conclude that isotropic evaporation occurs from the multi-crystal face surfaces for $P \lesssim 2 \times 10^{-8}$ torr.

b) Effect of Oxygen

In order to determine the effect of O_2 on the evaporation rate, either air or oxygen was leaked into the vacuum chamber during evaporation. The quantitative results of this investigation for O_2 are given in Figure 4 for 1×10^{-7} and 1×10^{-6} torr O_2. As expected, the presence of O_2 increases the evaporation rate due to the formation of volatile oxides. However, some interesting features of the O_2 effect were observed.

First, the effect of O_2 on the evaporation enhancement is greatest for the low temperature range. In fact, for $T > 1850$ K there is a negligible effect of O_2 on the evaporation rate. Secondly, at the highest O_2 pressure studied (1×10^{-6} torr), the rate of evaporation becomes independent of temperature for $1700 \lesssim T < 1800$ K. However, at 1700 K the evaporation rate increases ~ 32 times when the partial pressure of O_2 is increased from 2×10^{-8} to 1×10^{-6} torr.

c) Geometry Modification

Besides the increase in evaporation rate, the presence of a partial pressure of oxygen causes a significant alteration of the geometric shape as shown in Figures 5(b) and 6. With <100> oriented emitters after evaporation of 15 μm of LaB_6 in the presence of 1×10^{-7} torr of O_2, a pyramidal structure begins to form as shown in Figure 7. For the case of a 90° full angle cone it was found that the side facets of the pyramidal structure were (110) planes. On the other hand, the side facets of pyramidal structure formed from the 70° full angle cone are (111) planes as shown in Figure 6. It is readily shown that the (111) planes occur at this cone angle.

For some emitters, e.g. Figures 5(b) and 7, the conical emitter tip was polished to give a small flat of 30 to 50 μm in diameter. Figure 8 shows a before and after SEM photo after ~ 50 μm of evaporation from a truncated emitter. When measuring the evaporation rate of the truncated emitter, the rates of change of both flat size Δr_F and base radius Δr_B were determined (see Figure 9). In the case where the flat was a (100) plane the cylindrical portion of the emitter side contains four (100) planes spaced 45° apart. If one assumes that $\Delta r_F = \Delta r_B$, it can be shown that

$$\frac{\Delta r_s}{\Delta r_B} = \left[\tan\alpha + \frac{\Delta r_F}{\Delta r_B}\right] \cos\alpha \qquad (5)$$

where α is the cone half angle and Δr_s, as shown in Figure 9, is the evaporation rate from the side of the cone.

In Table I a summary of the evaporation data for the truncated, <100> oriented emitters is given along with the values of $\Delta r_s/\Delta r_B$ as calculated from Eq.(5).

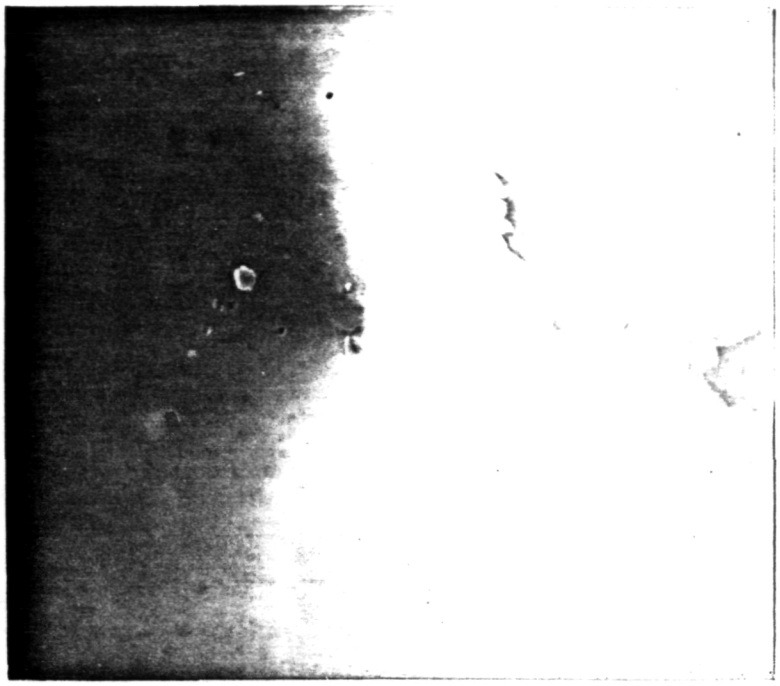

$\alpha = 90°$ $\Delta r = 62.5\,\mu m$ $P = 1 \times 10^{-8}$ torr

(a)

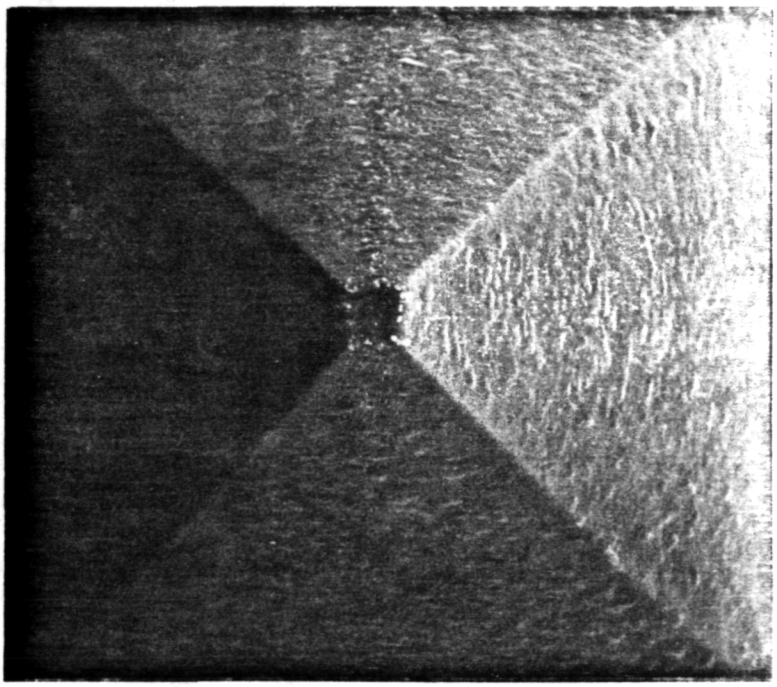

$\alpha = 90°$ $\Delta r = 63\,\mu m$ $P > 10^{-5}$ torr

(b)

Figure 5. SEM photos of the top view of <100> oriented LaB_6 cathodes after evaporation of 63 μm of material at the indicated pressures of O_2. The cone full angles were $\alpha = 90°$.

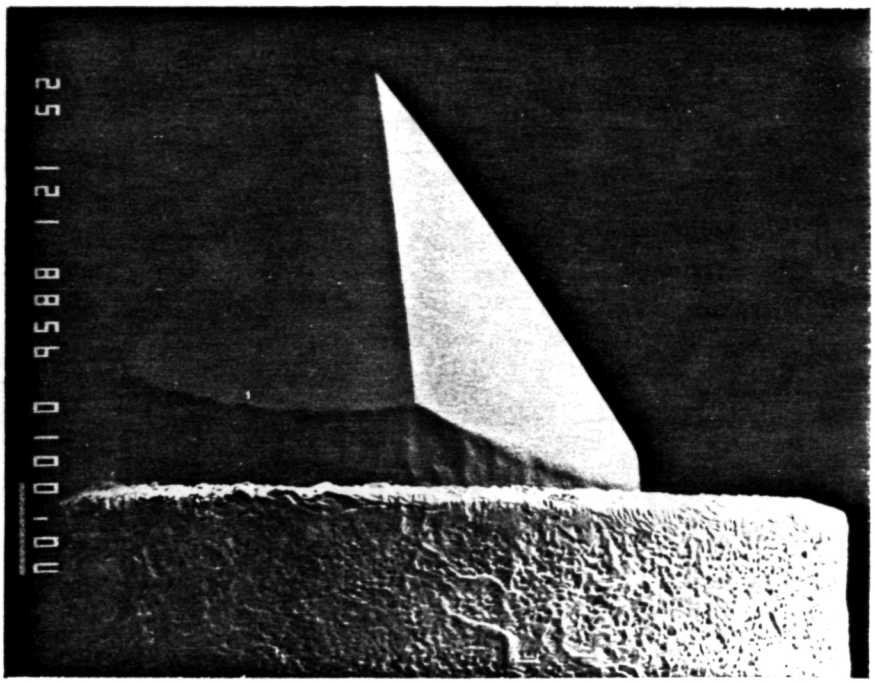

Figure 6. SEM photo of <100> oriented LaB_6 emitter after 500 hr at 1850 K in $10^{-7} < P < 10^{-6}$ torr of air. Thickness loss was 90 μm.

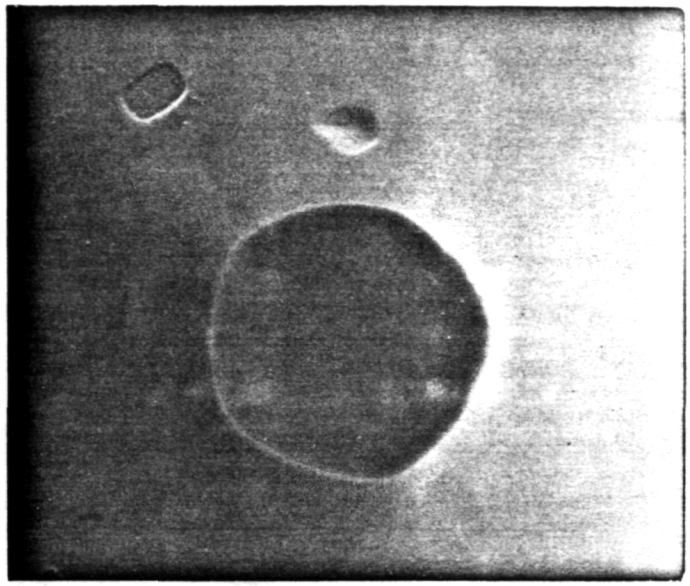

90°
(a)

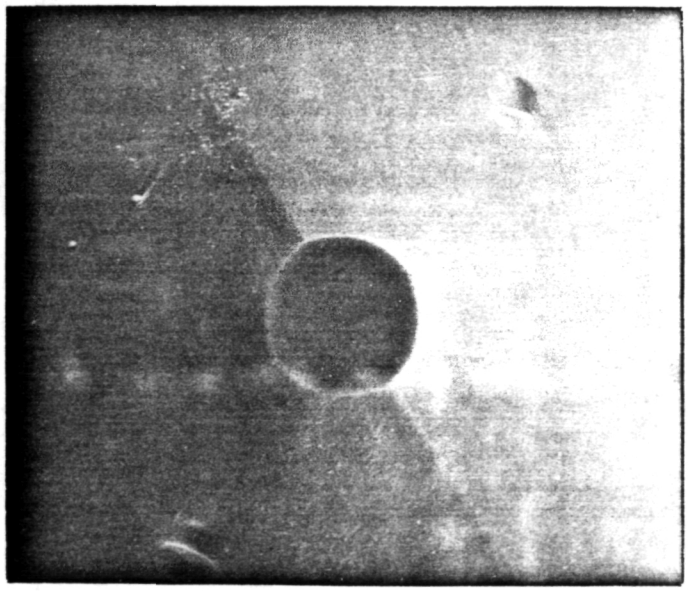

70°
(b)

20μm

$\Delta r = 15.3\,\mu m$ Time = 350 hrs T = 1850 K

$P_{air} = 1.0 \times 10^{-7}$ torr

Figure 7. Top view SEM photos of a 90° (a) and 70° (b) full angle cone LaB_6 <100> oriented emitter with truncation. Photos taken after 15 μm material loss by heating at 1850 K for 200 hrs at 7×10^{-8} torr and 150 hrs at 1×10^{-7} torr of air.

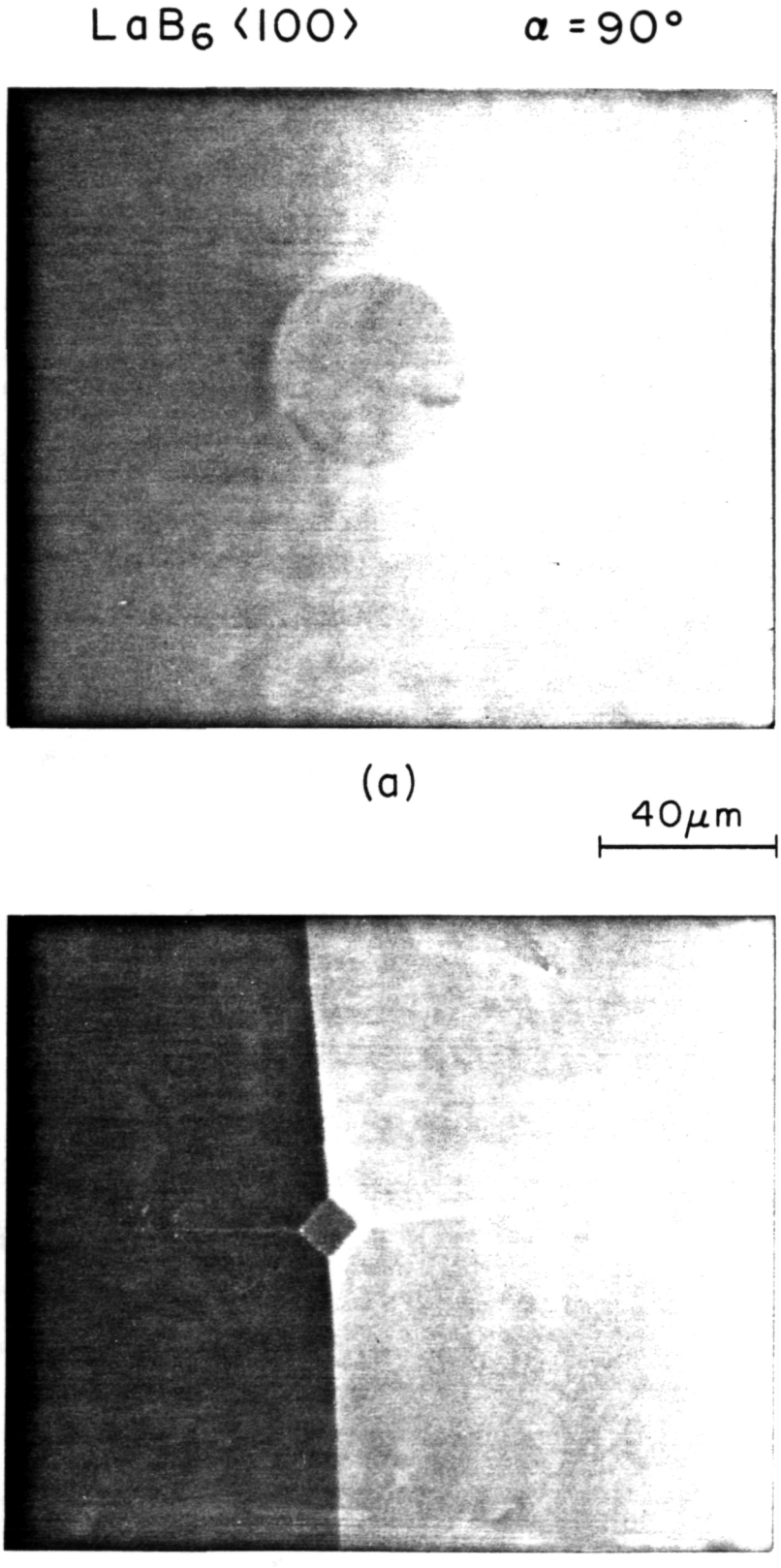

Figure 8. Top view SEM photos of a 90° full angle cone LaB_6 <100> oriented, truncated emitter before (a) and after (b) evaporation of 50 μm of material in 1×10^{-6} torr of O_2.

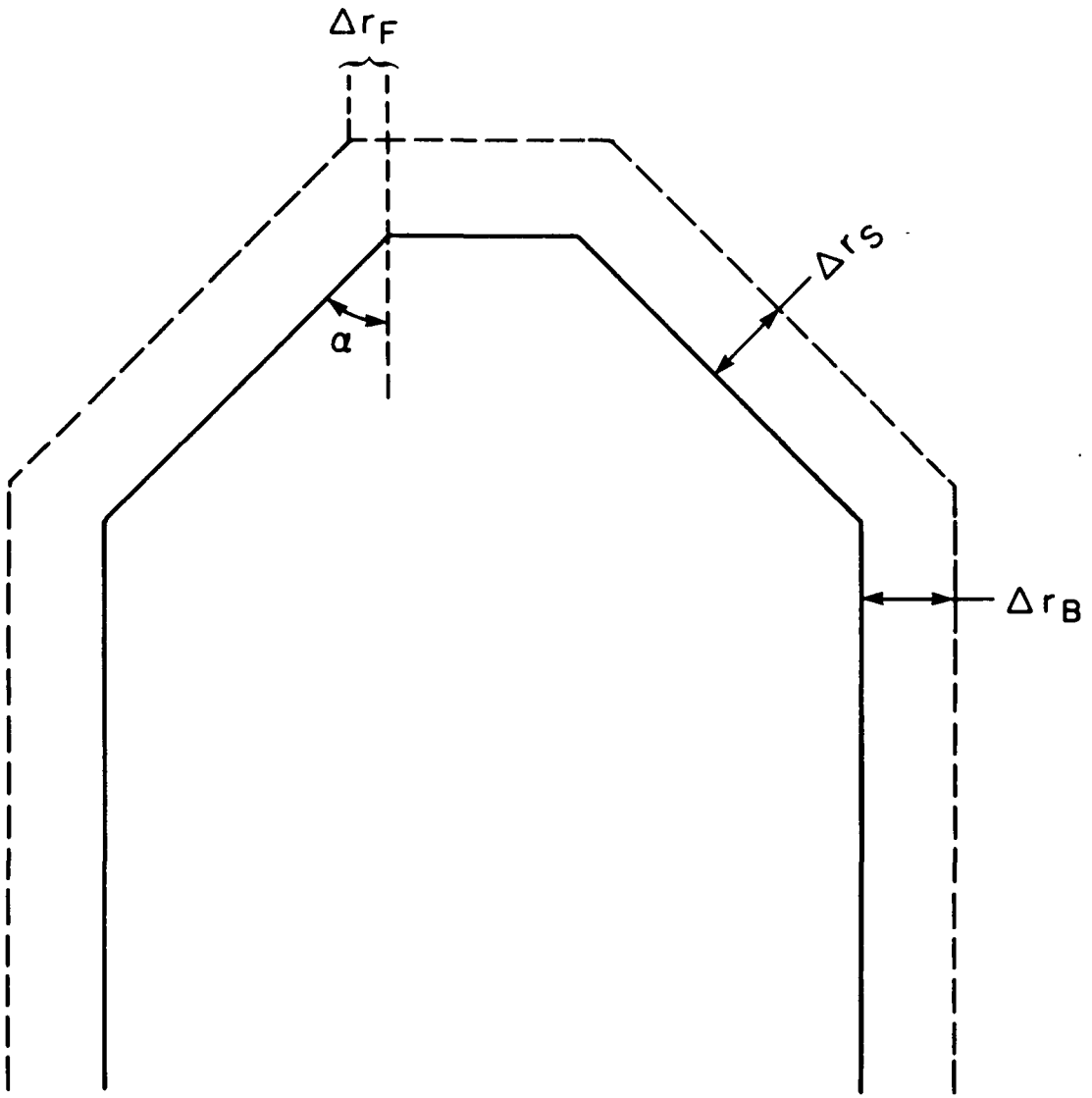

Figure 9. Diagram of geometric change measurements taken during evaporation of a truncated emitter.

TABLE I

Summary of evaporation data for the truncated, <100> oriented 70 and 90° full angle emitters of $LaB_{6.09}$ and $CeB_{6.2}$. The experimental and calculated values of $\Delta r_F/\Delta r_B$ and $\Delta r_s/\Delta r_B$, respectively, are given.

Emitter No.	Full Cone Angle (degrees)	P_{O_2} (torr)	$\Delta r_F/\Delta r_B$	$\Delta r_s/\Delta r_B$
19	90	1.2×10^{-8}	.286	.909
20	90	7×10^{-8}	.279	.904
23	90	1×10^{-7}	.273	.900
23	90	1×10^{-6}	.310	.926
23	90	1×10^{-6}	.320	.933
25	90	1×10^{-7}	.317	.931
21	70	1×10^{-7}	.472	.960
22	70	1×10^{-7}	.464	.954
24	70	1×10^{-7}	.471	.959
26*	70	1×10^{-7}	.468	.957

*$CeB_{6.2}$ all others are $LaB_{6.09}$

Note that the ratio of $\Delta r_F/\Delta r_B$ for the 70° emitter is ~ 27% larger than for the 90° emitter. Also, since the 70° and 90° emitters expose primarily (111) and (110) planes respectively on the sides of the emitter cone, one can deduce from the Table I results that

$$\frac{\Delta r_{110}}{\Delta r_{100}} = 0.917$$

$$\frac{\Delta r_{111}}{\Delta r_{100}} = 0.958$$

$$\frac{\Delta r_{110}}{\Delta r_{111}} = 0.957$$

Thus, the anisotropy in evaporation rates of the major crystal planes due to O_2 enhancement is

$$\Delta r_{100} > \Delta r_{111} > \Delta r_{110} \qquad (6)$$

The above observed O_2-induced anisotropy in evaporation rate is believed to be the cause of faceting. Figure 10 illustrates the observed profile angles of the 70° and 90° cone angle emitters. For the 70° cone angle emitter the observed (111) facets are separated by (110) ridges. On the other hand, the 90° cone angle emitter forms (110) facets separated by (211) ridges. In order for such faceting to occur the crystallographic anisotropy in evaporation rate must be as follows:

$$\Delta r_{111} > \Delta r_{110} > \Delta r_{211} \qquad (7)$$

This agrees with the observed variation in evaporation rate given in Eq.(6).

2. Emission Studies

Thermionic emission studies have been performed on flat cathode structures of the type shown in Figure 1. To date, thermionic work functions

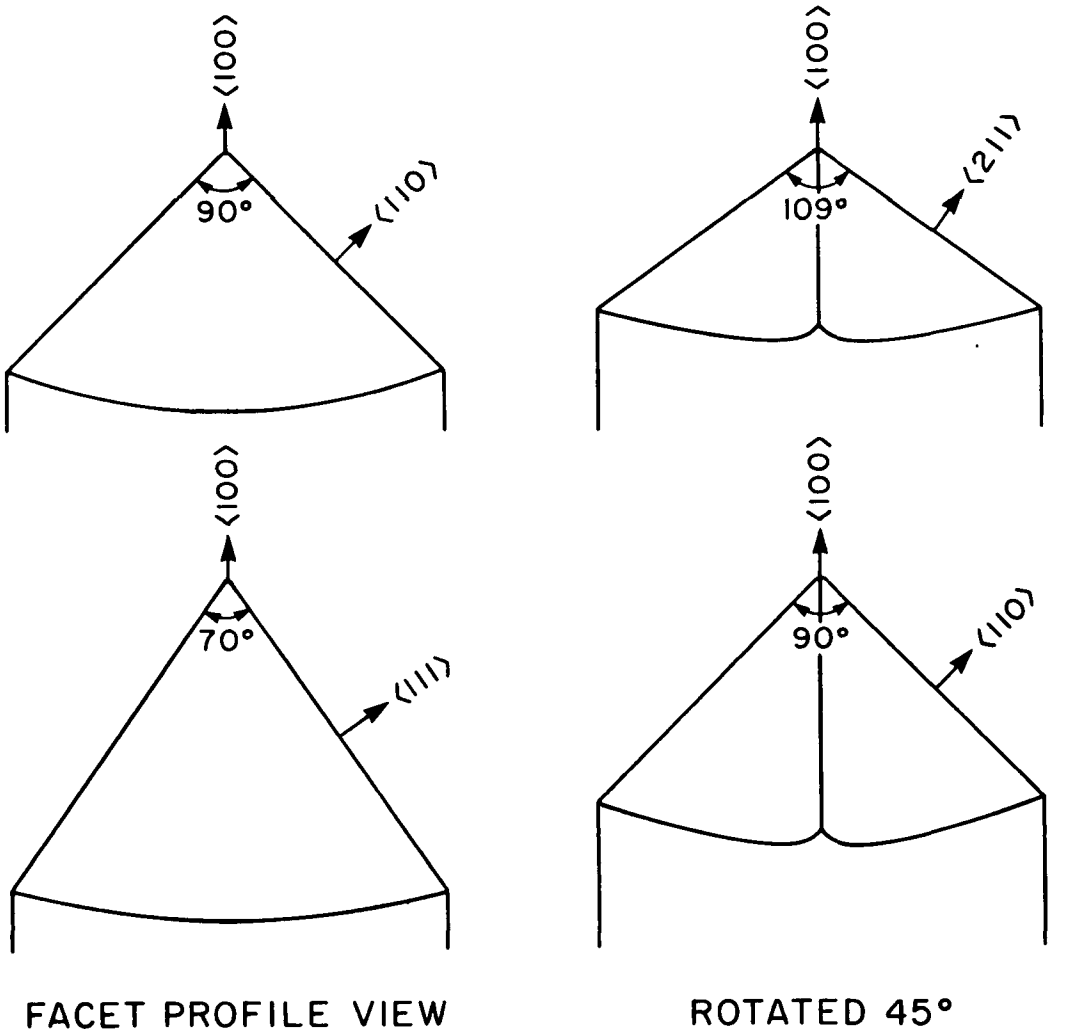

Figure 10. Profile of facet and ridge orientation for a 90° and 70° full angle cone of a <100> oriented emitter.

ϕ_e measured according to Eqs.(1) and (2) have been obtained as functions of T for the (210) and (310) planes of $LaB_{6.09}$. These results have been compared with the (100) planes as shown in Figure 11. Clearly the (210) and (310) planes exhibit much lower work functions than the (100) planes throughout the temperature range. In addition, the results suggest that $\phi(310) < \phi(210)$. The (310) crystal was operated for up to 120 hours with no change in work function.

Theoretical J(V) characteristics based on ideal diode performance and the (210) and (310) work function data are given in Figure 12. The current density J vs diode voltage V curves are based on Eqs.(1) and (2) when the emission is temperature limited and on the Childs law relationship

$$J \alpha d^{-2} V^{3/2} \tag{8}$$

in the space charge limited regime. The results of Figure 12 show a dramatic increase in J at the so-called "knee," i.e., the voltage at the transition between space charge and temperature limited emission. We shall call this "knee" current density J_s. For example, at 1700 K, J_s = 17 A/cm^2 for the (210) plane. Correspondingly the diode voltage for d = 0.1 cm must be increased from 600 to 1700 V in order to realize this increase in J_s.

The effect of changing diode spacing d on the J(V) characteristics is given in Figure 13 for the (210) crystal plane at 1700 K. Although the diode voltage of the "knee" shifts with d, the value of J_s remains constant at 17 A/cm^2.

Values of the (100), (210) and (310) work functions of LaB_6 were also measured at room temperature by the FERP technique. The results of the FERP and thermionic work functions are summarized in Table II. Both methods of

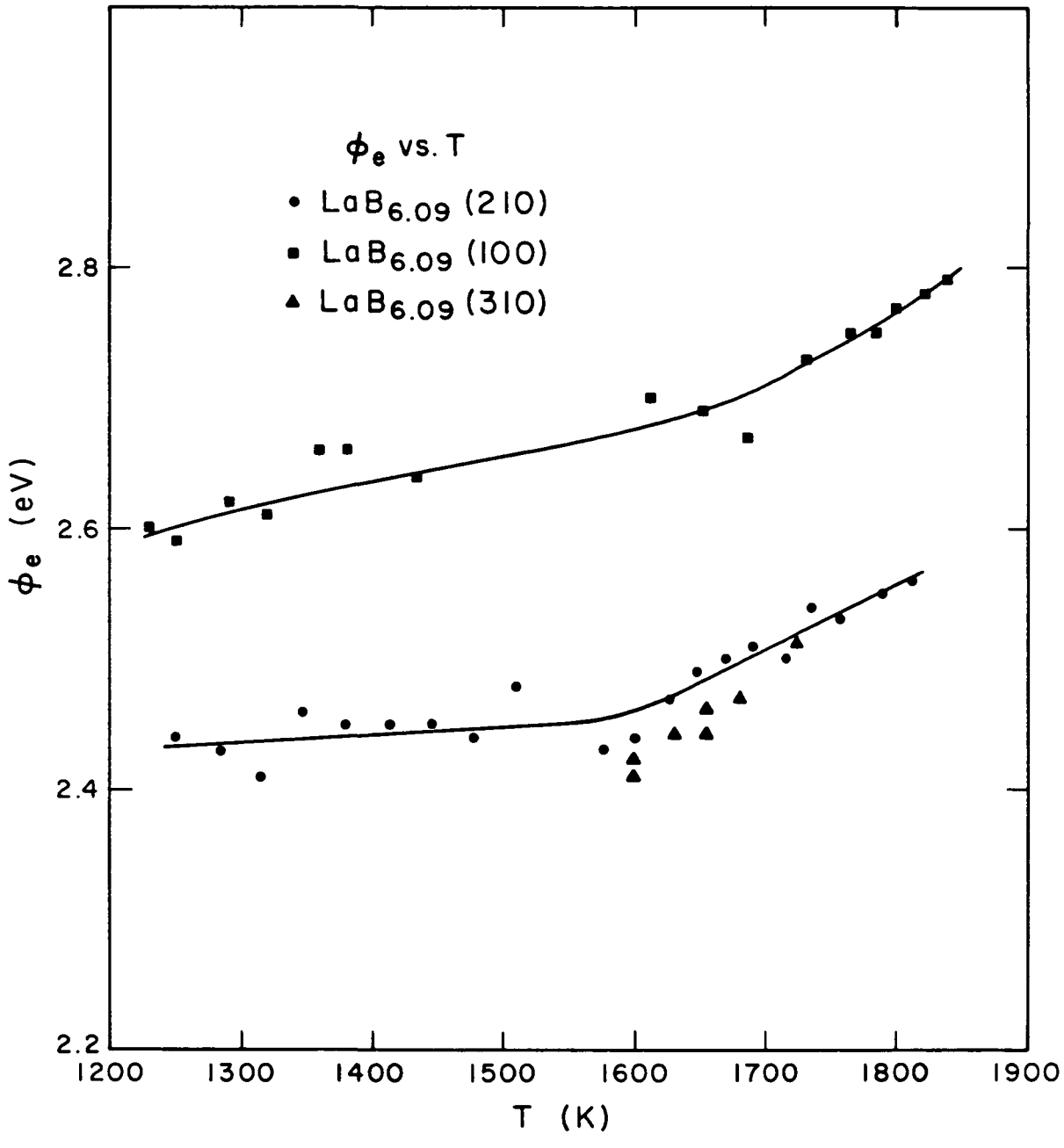

Figure 11. Results of thermionic work function ϕ_e vs T for the (100), (210) and (310) planes of $LaB_{6.09}$.

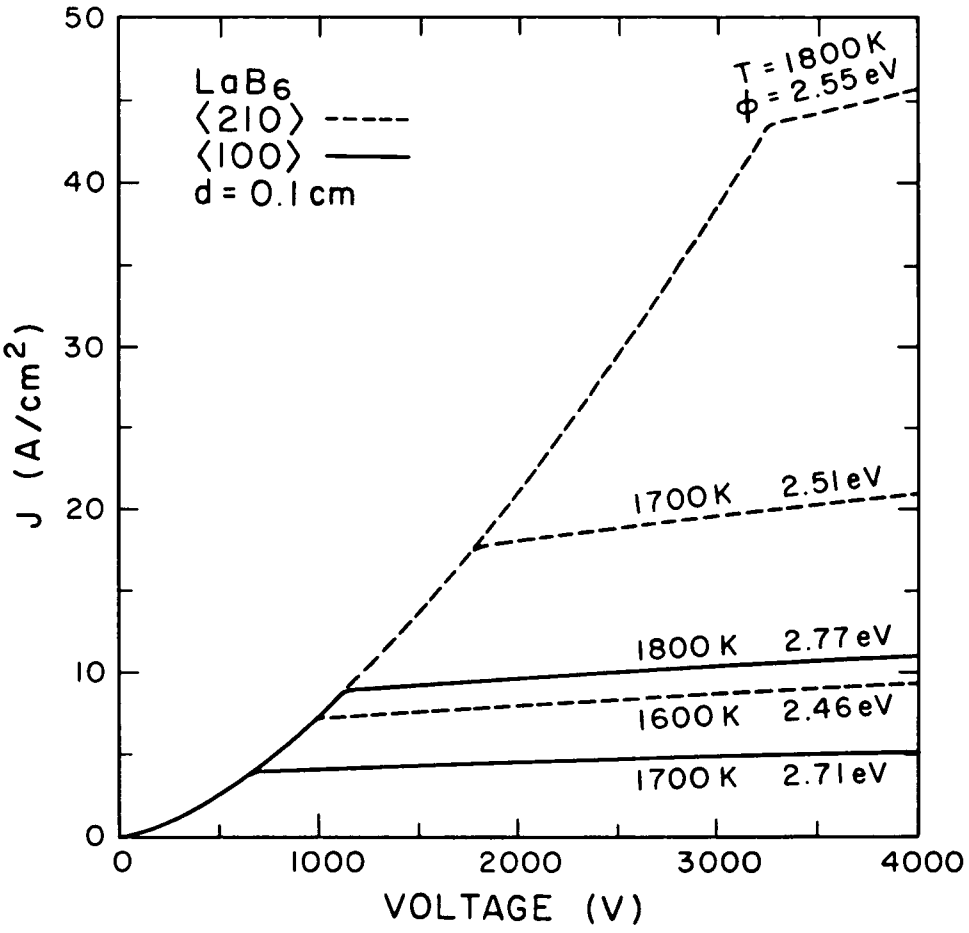

Figure 12. Theoretical plot of J vs diode voltage for a (210) and (100) LaB_6 emitter. Diode spacing d = 0.1 cm. The emitter temperature and work function are indicated.

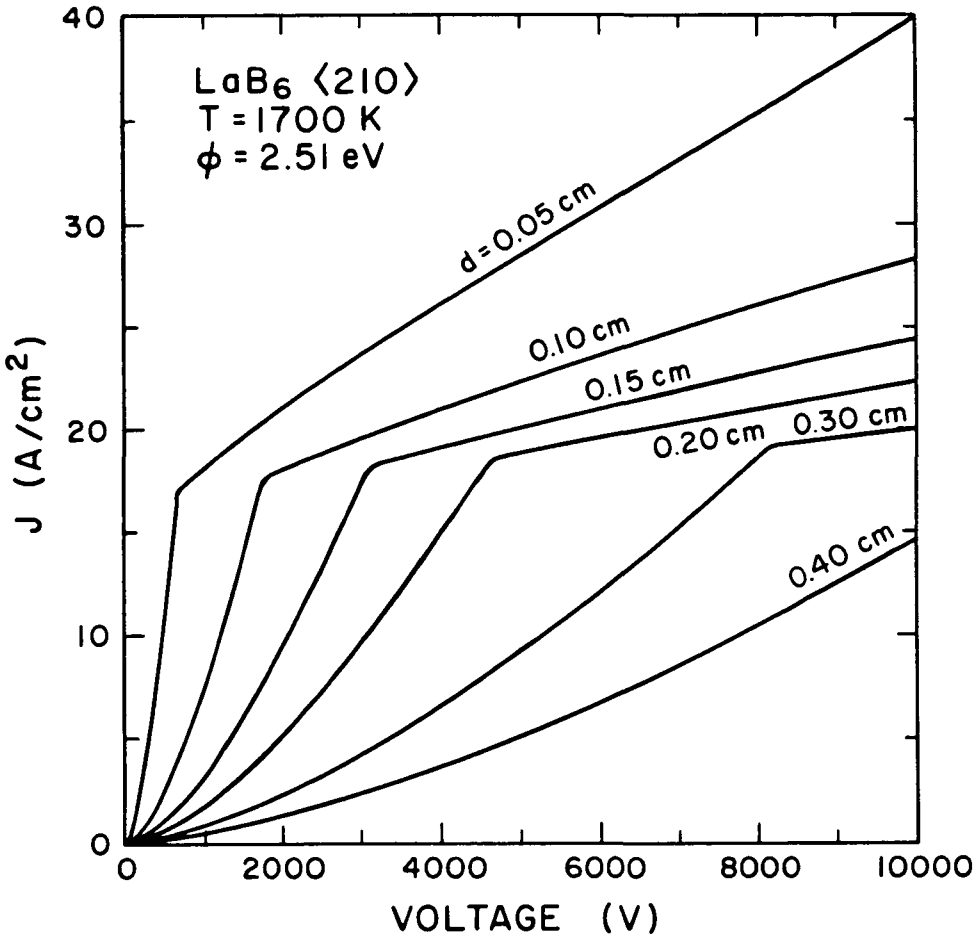

Figure 13. Theoretical plot of J vs diode voltage for a (210) LaB_6 emitter at the indicated temperature and diode spacing.

work function measurement agree that the (310) crystal face of LaB_6 exhibits the lowest value.

TABLE II

Summary of FERP (ϕ_F) and Zero-Field Thermionic (ϕ_e) Work Functions for $LaB_{6.09}$ Crystal Planes

Plane	ϕ_F (eV) (at 300 K)	ϕ_e (eV) (at 1600 K)
100	2.60 ± .05	2.52 ± .04
210	2.55 ± .05	2.46 ± .04
310	2.50 ± .05	2.42 ± .04

IV. Discussion and Conclusions

For traveling wave tube (TWT) applications it is desirable for the cathode to possess both a low work function and high heat of vaporization. In this way the cathode figure of merit, defined according to Eqs.(1) and (4) as J/R_T, can be maximized. For a specified J a low value of work function will allow the cathode to be operated at low temperatures, thereby reducing heating power and the attendant tube problems. Also, for a required cathode operating temperature it is desirable to minimize evaporation of cathode material since a reduction of cathode life and an increase in grid emission problems are associated with high volatility.

In Figure 14 the temperature dependence of J and R_T are summarized for LaB_6(310), (210) and a state-of-the-art impregnated dispenser cathode (IDC). The evaporation rate used in Figure 13 for LaB_6 was that measured for $P \lesssim 2 \times 10^{-8}$ torr. It is important to note that J/R_T for the LaB_6(310) cathode exceeds that of the IDC over the entire range of J and T in which IDC's can be operated with reasonable life. With our present understanding, the main limit on life of the LaB_6(310) cathode is dimensional change due to evaporation. However, according to Figure 14 a LaB_6(310) cathode can be expected to give $J = 13\ A/cm^2$ at a temperature of 1700 K where the evaporation rate is only 20 μm/year. The IDC would not be able to operate at such a value of J because of excessive evaporation and limited operating life. Any advantage of the IDC seems to be outweighed by the lower vaporization expected from the LaB_6(310) and the high reproducibility of single crystal fabrication. Thus the LaB_6(310) cathode appears ideal for long lifetime, high current density TWT's.

V. Future Work

During the remaining half year of the current program the LaB_6(310) crystal plane will be investigated with respect to current density stability. In particular, life tests of J vs time at various temperature and pressures of background gases will be carried out.

In addition, two LaB_6(310) flat cathodes of the type shown in Figure 1 will be constructed for evaluation in a gun structure being designed at the University of Utah for a BWO TWT. Communications between OGC and University of Utah personnel on this matter are in progress. It is expected that such cathodes will be delivered by April 15, 1984.

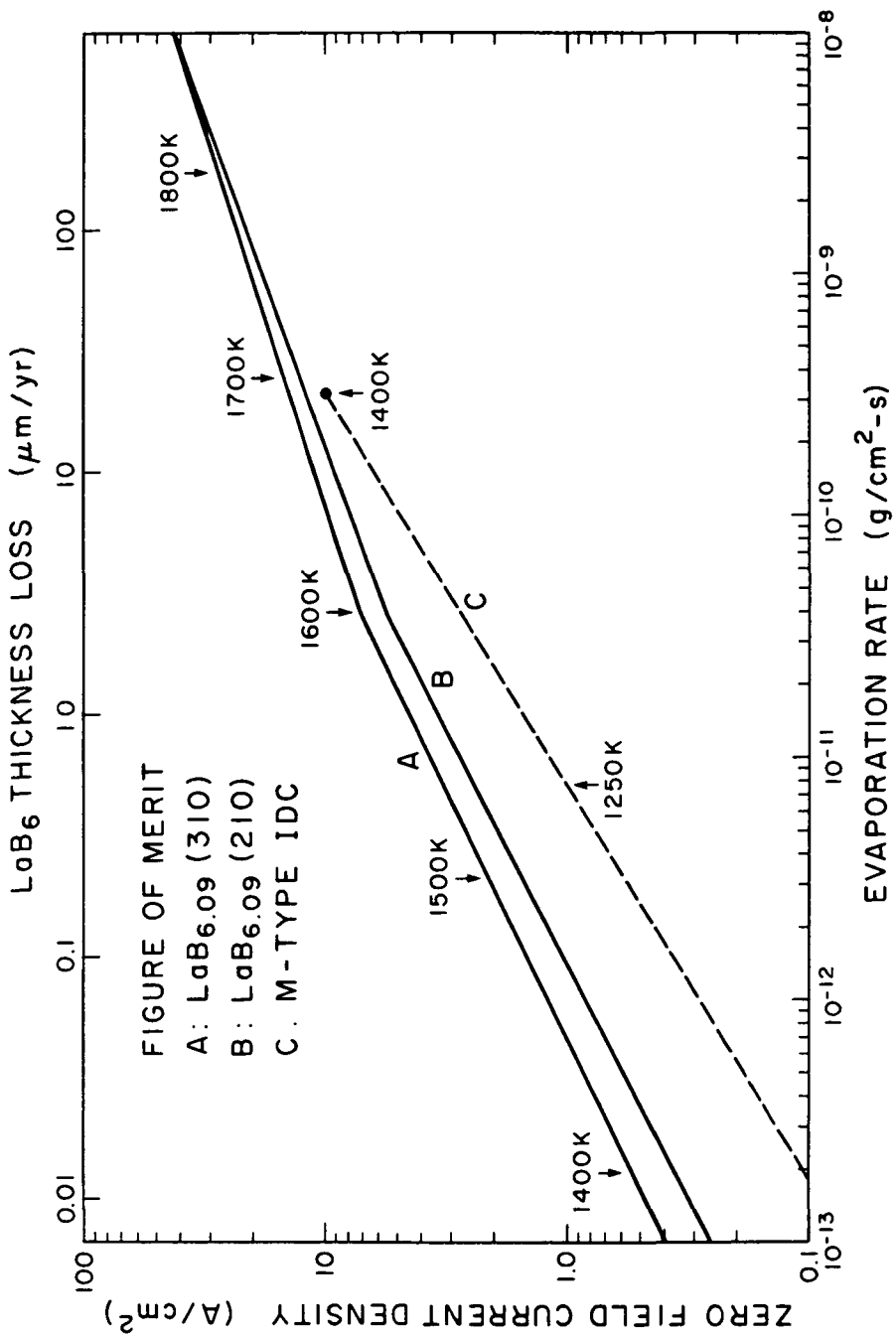

Figure 14. Figure of merit comparison (J/R_T) of LaB_6(310) and (210) faces and a state-of-the-art impregnated dispenser cathodes (IDC).

References

1. E. Gibson and J. Verhoeven, J. Phys. E8, 1003 (1975).
2. L. W. Swanson, M. A. Gesley and P. R. Davis, Surf. Sci. 107, 263 (1981).
3. E. Storms, J. Appl. Phys. 50, 4450 (1979).
4. R. Strayer, W. Mackie and L. Swanson, Surf. Sci. 34, 225 (1973).
5. P. R. Davis and S. A. Chambers, Appl. Surf. Sci. 8, 197 (1981).

APPENDIX I

A Determination of the Low Work Function Planes of LaB_6

by

M. Gesley and L. W. Swanson

Oregon Graduate Center

19600 N.W. Walker Road

Beaverton, Oregon 97006

ABSTRACT

A study of the temperature and orientation dependence of the field ion and electron emission and the average work function for a LaB_6 emitter have been carried out between 77 and 1800 K. These results indicate that the (310) surface is thermally stable and has the lowest work function of any single crystal plane of LaB_6. This result is confirmed by field emission retarding potential (FERP) work function (ϕ) measurements at 300 K which gives $\phi(310)$ = 2.50 eV. The results show that the relative orientation dependence of the room temperature work function is $\phi(310) < \phi(210) < \phi(100) < \phi(110) < \phi(111) < \phi(211)$. This ordering is in accordance with the relative dipole contribution to the work function when surface reconstruction is included. The orientation dependence of the field electron emission is sensitive to field evaporation, thermal equilibration, and carbon contamination.

I. Introduction

In the development of a high brightness electron source considerable attention has been focused on the crystallographic dependence of the work function of LaB_6. For the low index planes the orientation dependence of the work function has been determined by thermionic emission (TE) [1,2], field emission retarding potential (FERP) [1], and photoelectric [3] methods to be $\phi(100) < \phi(110) < \phi(111)$. Many studies have focused on the low index planes due to their thermal stability and ease of fabrication. Field-ion microscopy (FIM) has presented direct visual evidence of this stability on an atomic scale [1,4]. However several studies have indicated that certain high index planes may exhibit even lower work functions and thermal stability (i.e., stability with respect to macroscopic surface reconstruction). A TE study measured a 2.41 eV work function for the (346) plane [1]. An ultraviolet photoelectron study (UPS) measured a 2.2 eV work function for the (210) plane [5]. Another TE study found $\phi(210) < \phi(100)$ [2].

In this study field emission microscopy (FEM) and FIM studies of LaB_6 have been carried out as a function of temperature to investigate the possible existence of high index, low work function planes which are stable at high temperatures. The combined use of FIM and FEM allows one to qualitatively discern the crystallographic dependence of work function from local electric field variations. Auger electron spectroscopy (AES), FERP, and TE measurements on macroscopic single crystals have also

been performed in order to verify that the relative ordering of work function is: $\phi(310) < \phi(210) < \phi(100) < \phi(110) < \phi(111) < \phi(211)$. Measurements of the work function and FEM patterns of an originally field evaporated emitter as a function of annealing temperature, and studies on macroscopic samples using FERP and AES, indicate that low work function surfaces generally correspond to a higher surface concentration of lanthanum atoms. In a similar study concerning the temperature dependence of the FIM and FEM patterns carried out by Futamoto et al [4] symmetric field emission patterns were only obtained in the range of 1700 K < T < 1950 K. To obtain reproducible and coherent FEM patterns over the entire range of temperatures requires a combination of high vacuum ($< 10^{-9}$ torr) and beginning with a low temperature field evaporated surface. Our results indicate that the FEM pattern is sensitive to certain ambient gases and that raising the temperature of the crystal to 1900 K is an insufficient method for removing surface carbides.

II. Experimental

The macroscopic samples of LaB_6 were obtained from a single crystal rod (1.0 mm diameter) prepared by a float zone melting technique described by Gibson and Verhoeven [6]. Single crystal stoichiometry was determined by chemical analysis. Crystal mounting procedure and heating configuration have been explained previously [1]. Measurements made on macroscopic single crystal

surfaces were carried out in an ULTEK TNB-X 250 l/s ultra-high vacuum system containing a Physical Electronics CMA Model 10-155 Auger Electron Spectrometer, FERP gun for room temperature work function measurements, and an outgassable guard ring anode for obtaining thermionic work functions. The AES measurements were performed with a 10 μA primary beam current with 5 kV beam energy. Quantitative analysis of the AES data used the peak-to-peak heights of the derivative of the N(E) curve with one volt modulation. The thermionic (ϕ_e) and FERP (ϕ_F) work function measurements have been described in detail else-where [1,7]. Both AES and work function measurements were carried out after heating the crystal in excess of 120 hours at 1800 K.

The FIM and FEM studies were performed in a standard, low temperature (77 K) microscope using a microchannel plate to intensify the hydrogen or helium ion image and the field electron image. The bakeable, ultra-high vacuum system had a base pressure of 5×10^{-10} torr. Image gas pressures for FIM studies were typically 1×10^{-4} torr and all FEM work was performed below 1×10^{-9} torr. Field evaporation of LaB_6 in the presence of H_2 occurs slowly at 220 MV/cm which is near the best image field (BIF) for H_2 image gas. In contrast, the field evaporation of LaB_6 in the presence of a noble gas or in vacuum occurs at 420 MV/cm.

The microscopy studies employed needle-like LaB_6 crystals obtained from the molten Al solvent method described by Futamoto

et al [8]. During the course of the microscopy study and subsequent analysis of the literature it became apparent that small concentrations of surface contaminants could drastically alter the emission distribution. In order to avoid this possibility the emitter was first heated to 1650 K ($P < 1 \times 10^{-9}$ torr) in order to remove adsorbed CO, H_2O, and O_2 from the emitter shank and support assembly and then field evaporated to remove any compounds remaining on the surface of the emitting area. The starting point for all of the FIM and FEM experiments was thus an emitter with a field evaporated surface free of any shank contaminants that could migrate to the emitting area during higher temperature annealing.

III. Results

A. FEM/FIM Results

Beginning with a clean, field evaporated LaB_6 emitter FIM and FEM images were obtained at 77 K along with a measurement of the total field emission current(I) as a function of applied voltage (V) after heating the sample for two minutes in 100 K increments. The slope (m) of the Fowler-Nordheim (FN) plot of the I(V) characteristic is given by

$$m = d[\ln (I/V^2)]/d(1/V) = b\phi^{3/2}/\beta \qquad (1)$$

where ϕ is the average emitter work function, $\beta = F/V$, F is the electric field at the emitter surface and b is a constant. The variation in FN slope with annealing temperature is shown in

Figure 1. The error bars correspond to the variation between two experimental runs. The best image voltage (BIV) for the H_2 FIM image at 77 K, was constant over the range of emitter annealing temperatures implying that β in Eq.(1) remained unchanged during the course of the temperature processing. By expressing the electric field in the approximate form

$$F = V/kR, \qquad (2)$$

where R is the emitter radius and k is a geometrical factor with values between 4 and 8 depending on the emitter shape [9], then from Eqs.(1) and (2) $\beta = (kR)^{-1}$. The relationship $V_{BIV} \propto R$ for a constant F is verified in Figure 2 where the emitter radius was calculated by the ring counting method [9] between the (110) and (210) planes for several different emitter radii. Given that β and hence R remained constant during the course of the temperature processing, the changes in the FN slope must be interpreted as variations in the average emitter work function.

For each point on the graph in Figure 1 corresponding FIM and FEM images were obtained. Representative micrographs, which were reproducible within a range of 100 K, are shown in Figure 3. Beginning with a H_2-field evaporated surface shown in Figure 3(a) and (a') no significant change was found in the FEM image until approximately 725 K, and not in the FIM pattern until 1000 K. Figure 1 indicates that for $T < 800$ K the average work function increases with temperature. The fact that the FIM image remains unchanged with respect to the 77 K field evaporated surface indicates that La and B

diffusion are inconsequential for T < 1000 K and that the initial increase in the average work function with temperature must be attributed to local surface atom rearrangement.

Figure 3(b') shows that heating for two minutes at 910 K results in enhanced electron emission from the {110} regions. The average work function begins decreasing at this point although it still exceeds the value for the original evaporated surface at 77 K. At 1295 K the (110) planes are no longer resolved as shown in Figure 3(c). The electron emission becomes more uniform (see Figure 3(c'), and the average work function undergoes a rapid decrease.

Heating the sample in the range 1355 K < T < 1770 K results in a dramatic change in the FEM image (see Figures 3(d) to 3(f) and a sharp reduction in the average work function. In addition, the FIM patterns show a growth of the {111}, {110}, {112} and to some extent the {100} planes. As the temperature increases towards the upper part of the stated temperature interval bright emission, initially observed from the {210} planes, proceeds to the {310} planes. Evidence indicating that $\phi(310) < \phi(210)$ can be obtained from Figure 3(f) by carefully noting the positions of these planes from the FIM patterns. Field enhancement is centered on the {210} planes as shown by Figure 3(f) whereas the enhanced electron emission is centered more on the {310} planes. Although the FIM image Figure 3(f) shows some field enhancement in the {210} - {310} regions, the BIV was unchanged indicating the average value of

emitter radius remained constant throughout the annealing process. Thus the large decrease in the FN slope at $T > 1355$ K must be attributed to a reduction in ϕ with the {310} planes exhibiting the lowest work function for the thermally annealed end form.

Several previous studies have reported that enhanced field emission occurs in the (211) region (Ref. 1, Fig. 6(d); Ref. 4, Fig. 2(a); Ref. 10, Fig. 4) for an emitter heated at $T \sim 1800$ K. Our studies show that this emission distribution is obtained by heating in the presence of hydrocarbons. Oxygen was ruled out as a contaminant as its compounds would be removed by heating at this temperature, carbon however is not [1]. Only by field evaporation of the emitter followed by heating in high vacuum ($< 10^{-9}$ torr) could we reproducibly obtain the Figure 3(f') pattern. Comparing FN slopes from the carbon contaminated emitter, which resulted in bright emission from the {211} planes, with the FN slope corresponding to the {310} emission shows: $m(211)/m(310) \simeq 1.3$. This is consistent with FERP and AES measurements which indicate that a small amount of surface carbon significantly increases the work function [1].

B. Macroscopic Single Crystal Results

Room temperature FERP work function measurements on macroscopic single crystals, summarized in Table I, are consistent with the present field emission results which indicate that $\phi(310) < \phi(210) << \phi(211)$. In fact the (211) plane appears to have one of the highest work functions of all measured planes. The TE work function measurements are generally 0.1 eV less than the FERP values for a given plane.

Figure 4 shows the temperature variation of the effective TE work functions for the (100), (210) and (310) planes. The ϕ_e values for the (310) plane, although taken over a limited temperature range, are slightly lower than the ϕ_e values for the (210) plane. For both the (310) and (210) planes no change in work function was observed upon heating at 1800K for 120 hours.

In another experiment a LaB_6 crystal was cleaved along a (100) plane in ultra-high vacuum and examined by AES. Table II summarizes the AES results for the cleaved and annealed LaB_6(100) surfaces.

IV. Discussion

An indication of the nature of the H_2-field evaporated surface can be obtained by considering the slope of the graph in Figure 2. The value of the slope (equal to kF) coupled with an estimate of the hydrogen best image field-BIF of 220 MV/cm [9] results in a geometrical factor k = 6. This result is obtained by assuming the observed step height employed in the ring counting method is equal to the lattice constant a_o = 4.14 Å of LaB_6. Using a step height value of $a_o/2$ implies k = 12 whereas a value of $2a_o$ results in k = 3, both of which are outside the typical range of values for the geometrical factor. Since the net plane rings observed in the FIM correspond to ledge atoms, a step height equal to the lattice constant implies that only one atomic species exists at the ledge sites (except for a nonpolar plane such as an unreconstructed (110)). This conclusion was also arrived at in an earlier FIM study using noble gases to image rare-earth hexaborides [11].

A question of interest is, which element is being imaged by FIM? Futamoto and Kawabe [11] argue that the FIM image of a field evaporated surface is a result of La-atoms only. Their argument is based on the idea that the ionization probability is greater above the La-atom due to the charge transfer from the La-atom to the B_6 octahedra. But this argument depends on the assumption that either the B_6-octahedra and the La-atom exist in equivalent sites or that lanthanum is outermost on the low index planes of the field evaporated surface. The first possibility cannot hold geometrically for the (100) plane, one which is visible in the FIM for both hydrogen and helium field evaporated endforms [1]. The second possibility contradicts both the results of atom probe studies on surfaces field evaporated with noble gases [12] and the results presented here.

In a detailed study of the field evaporation of the LaB_6(100) plane in the presence of noble gases carried out by Murakami et al.[12] only boron was observed to field evaporate from the central region of the net plane, whereas both La and B field evaporated at the net plane edge. The authors concluded that field evaporation in noble gases or vacuum proceeds by decomposition of the boron octahedra with partial removal of boron atoms followed by simultaneous evaporation of the lanthanum atom and the remaining boron atoms from the decomposed octahedra. Thus, upon field evaporation the polar (100) face always results in a configuration with boron outermost. The alternative

possibility of having lanthanum outermost, caused by initial evaporation of lanthanum ions with simultaneous decomposition and partial removal of boron atoms from the B_6-octahedra, then followed by evaporation of remaining boron atoms, is unlikely due to the difference in the boron and lanthanum field evaporation rates.

It has been reported that at the stoichiometric composition the sublimation energies of B and La are equal [13]. Thus, one can show from the image hump field evaporation model [9] that under conditions of uniform work function and field strength that the difference in activation energies Q for field evaporation of La and B is

$$Q_B - Q_{La} = I_{B^+} - I_{La^+} = 2.68 \text{ eV} \qquad (2)$$

where I_{B^+} and I_{La^+} are the respective first ionization potentials. This implies that in vacuum or in the presence of noble gases La will be field evaporated at a much higher rate than B from an initially thermally equilibrated surface. The evaporation field is significantly reduced by H_2, as discussed previously, presumably through boron hydride formation [14]. Nevertheless, in view of the near equality of the BIV, FN slopes and, hence, work function [1] for the emitter field evaporated in either H_2 or He image gas environments, we conclude that both surfaces are similarly boron rich and that the observed step

heights used in Figure 2 are due to the presence of boron in the ledge sites with the possible exception of the nonpolar {110} planes where both lanthanum and boron may exist.

The present experiments indicate that field evaporation generally leaves a boron rich surface and that subsequent heating at T ~ 1800 K results in a low work function (310) surface caused by diffusion of La-atoms to the surface either from the emitter shank or from the underlying bulk without a large change in the average emitter radius. This model is supported by three independent experiments.

First, a comparison of the AES result of the fractured and annealed (100) surfaces summarized in Table II shows that the La(78 eV)/La(625 eV) ratio increases upon heating at 1700 K. Because the 78 eV Auger electron has a shorter escape depth than the 625 eV electron the increase in the La(78 eV)/La(625 eV) ratio implies an increase in the surface La-concentration upon annealing. If we assume the surface structures of the field evaporated and fractured surfaces are similar and represent a nonequilibrium surface, i.e. no surface reconstruction, then it can be concluded that the large reduction in m (or ϕ) observed in Figure 1 at ~ 1400 K is due to an increase in surface lanthanum concentration.

Secondly, in a time of flight atom probe study a marked increase in the La/B ratio occurred when heating an originally field evaporated emitter at or above 1400 K for five minutes in

vacuum [15]. As shown in Figure 1, this also is the temperature where the average emitter work function undergoes a large decrease.

Finally, assuming the field evaporated surface has a work function equal to elemental boron ϕ_B = 4.6 eV [16], one may estimate the work function of the (310) surface from the slope of the FN graph for the field evaporated and annealed(1800 K) surfaces using

$$\phi(310) = \phi_B\left(\frac{m(310)}{m(evap)}\right)^{2/3} \qquad (3)$$

This results in $\phi(310) \sim 2.1$ eV. Although the TE and FERP measurements of $\phi(310)$ are ~ 0.4 eV higher than this estimated value, the calculation does show that the work function change between the field evaporated and annealed surface is large and on the order of 2.3 ± 0.2 eV and supports the idea that the field evaporated surface is boron rich.

Binary systems with cubic lattice structure, such as the rare-earth hexaborides, possess certain crystal faces, e.g. (210), (111), and (100) that are polar in nature and others, e.g. (110), which are non-polar provided surface reconstruction does not occur. Angle-resolved photo-electron spectroscopy (ARXPS) has also shown that for annealed LaB_6 surfaces the La-atom is outermost on the (100) face, and that the (111) and non-polar (110) faces are reconstructed by normal displacements of the surface lanthanum by 1.2 and 1.78 Å respectively [3]. The

unreconstructed and reconstructed surfaces are depicted in Figure 4 for the low index planes of LaB_6. According to the latter picture the La-atom is outermost on the (100) and (110) planes and parallel with the B_6-octahedra on the (111) face. Thus, the separation between the outermost lanthanum layer and the center of the B_6 plane is 2.1, 1.6, and 0.0 Å for the (100), (110), and (111) planes respectively. From Table I, which summarizes the work function and AES results for various crystal faces, one generally finds that the relationship between work function values and B/La ratios (based on the B(KLL)/La(MNN) AES ratio) is such that (excepting the (211) and (310) planes) the work function decreases as the surface lanthanum concentration increases.

Conclusions concerning the relation between the true surface concentration of lanthanum and boron and the measured AES ratios must be accepted with some caution as it is known that the latter are dependent on the Auger electron's exit angle [17], which may explain why the (211) and (310) planes are exceptions to the above-stated relation. Nevertheless the relative ordering of work function for the low index planes can be rationalized by considering the variation in the surface dipole contribution to the work function due to the position of the electropositive La-atoms relative to their nearest neighbor B_6-octahedra as seen in Figure 5.

This question can be addressed more quantitatively by assuming that the dipole moment due to the La-B chemical bond dominates the variation in the outer part of the work function $\Delta\phi_D$ with crystal face and is given by

$$\Delta\phi_D = 2\pi\mu\sigma_{La} \tag{4}$$

where σ_{La} is the surface atom density of the outermost La layer and the dipole moment μ per surface La atom is

$$\mu = \frac{ne}{j} \sum_{i=1}^{j} d_i \cos\theta_i \tag{5}$$

The dipole moment normal to the surface is obtained from Eq.(5) by considering the j nearest neighbor B_6 octahedra as a point negative charge of value ne where d_i is the La-B_6 distance and θ_i the angle of the La-B_6 bond with the surface normal. Thus, if one assumes the relative displacements of the La atoms given by reference 3 are correct it can be see from Table I that $\phi(100) < \phi(110) < \phi(111)$ is the order predicted by Eqs.(4) and (5).

If we momentarily assume there is no reconstruction of the (210) plane and compare $\Delta\phi_D$ for the (210) with the corresponding values for the (100), (110), and (111) planes (reconstruction included) it is found from Eq.(4) that the orientation dependence of the dipole contribution is $\Delta\phi_D(100) < \Delta\phi_D(210) < \Delta\phi_D(110) < \Delta\phi_D(111)$, assuming unit charge transfer per dipole, i.e., n = 1 in Eq.(5). Reconstruction of at least some of the lanthanum atoms on the (210) plane is suggested by ARXPS results that indicate La-atoms are outermost on the (210) and that they float slightly out of their positions [5]. In addition LEED results show a (1 × 1) pattern for the (210) indicating the surface atoms

are in registry with the bulk [5]. A proposed reconstruction consistent with the above data can be obtained by moving the La-atom nearest the B_6-ledge along the [120] direction to the plane intersecting the B_6-octahedra on the (210) plane (see Figure 5). This results in an increased dipole moment per unit area. The orientation dependence of the surface dipole contribution as given in Table I is then $\Delta\phi_D(210) < \Delta\phi_D(100) < \Delta\phi_D(110) < \Delta\phi_D(111)$ which is consistent with the orientation dependence of the work function measured by FERP and TE methods.

The dipole model overestimates the relative work function change between the various surfaces as shown in Table I. This effect has also been considered by Watson and Perlman [18] who note that surface ionic charge modification probably occurs in most polar crystals as this reduces the crystal capacitive potential energy. On this basis it is reasonable to consider a reduction in the assumed dipole charge of n = 1. For example, if n = 0.1 is used the predicted work function differences among the various planes are of the same order of magnitude as those measured.

In spite of the inability to properly specify the surface ionic charge the dipole model does indicate that the orientation dependence of the surface dipole moment, as surmised from geometrical considerations, plays an important role in determining the crystallographic variation of the work function. Most importantly, the dipole model does predict that the reconstructed

(210) plane has a lower work function than the major low index planes.

From the size of the net plane facets, the FIM pattern of the thermally annealed end form shown in Figure 3(f) indicates that the {110}, {111}, {112} and to some extent the {100} planes are the most thermodynamically stable planes. The absence of the {310} plane facets in Figure 3(f) may be interpreted that they are thermally unstable with respect to macroscopic, surface restructuring to lower index planes. At this juncture the main evidence that this is not so is the fact that no change in the high temperature thermionic or room temperature FERP work functions were observed upon heating a macroscopic (310) crystal at 1800 K for 100 hours.

IV. Conclusions

The crystallographic dependence of the work function of LaB_6 is determined by the relative concentration of lanthanum in the outermost surface layer and the dipole moment per surface La-atom. Surface reconstruction due to thermal equilibration and field evaporation can greatly alter lanthanum concentration and thus change the work function of specific planes. For example, the difference in ϕ for the boron-rich field evaporated surface and lanthanum-rich thermally annealed surface is ~ 2.3 eV. Retarding potential and thermionic work function measurements on macroscopic single crystals show the (310) plane to have the lowest work function which is almost 0.2 eV lower than the (100) plane value. Based on this work, a crystallographic map of the work function distribution can be derived as shown in Figure 6. It is found that the relative order of the work function for various faces is $\phi(310) < \phi(210) < \phi(100) < \phi(110) < \phi(111) < \phi(211)$. This order can also be derived on the basis of the relative dipole layer contributions using the respective reconstructed surfaces. It has also been found that the field emission distribution is extremely sensitive to contaminants and requires careful experimental procedures to properly interpret the information obtained.

Acknowledgements

This work was supported in part by contract F19628-80-C-0117 from the Electronics System Division of Hanscom AFB and by grant NAG 3-434 from the NASA-Lewis Research Center. The authors are grateful to Drs. Paul Davis and Joe Hutta for helpful discussions during the course of this work and to Mr. Noel Martin who fabricated the LaB_6 single crystals.

References

1. L. W. Swanson, M. A. Gesley, and P. R. Davis, Surf. Sci. 107 (1981) 263.
2. C. Oshima, M. Aono, T. Tanaka, S. Kawai, R. Shimizu, and H. Hagiwara, J. Appl. Phys. 51 (1980) 1201.
3. R. Nishitani, M. Aono, T. Tanaka, C. Oshima, S. Kawai, H. Iwasaki, and S. Nakamura, Surf. Sci. 93 (1980) 535.
4. M. Futamoto, S. Hosoki, H. Okano, and U. Kawabe, J. Appl. Phys. 48 (1977) 3541.
5. C. Oshima, M. Aono, T. Tanaka, R. Nishitani, and S. Kawai, J. Appl. Phys. 51 (1980) 997.
6. E. Gibson and J. Verhoeven, J. Phys. E 8 (1975) 1003.
7. R. Strayer, W. Mackie, and L. Swanson, Surf. Sci. 34 (1973) 225.
8. M. Futamoto, T. Aita, and U. Kawabe, Japan. J. Appl. Phys. 14 (1975) 1263.
9. E. W. Muller and T. T. Tsong, Field Ion Microscopy (American Elsevier, NY, 1969).
10. R. Shimizu, Y. Kataoka, T. Tanaka, and S. Kawai, Japan. J. Appl. Phys. 14 (1975) No. 7.
11. M. Futamoto and U. Kawabe, Surf. Sci. 93 (1980) 1117.
12. K. Murakami, T. Adachi, T. Kuroda, S. Nakamura, and O. Komoda, Surf. Sci. 124 (1983) 125.
13. E. Storms and B. Mueller, J. Phys. Chem. 82 (1978) 51.
14. S. Nakamura, Y. S. Ng, T. T. Tsong, and S. B. McLane, Jr., Surf. Sci. 87 (1979) 656.

15. T. Sakurai, G. Robertson, and Y. Kuk, Proc. Electrochem. Soc. 80-1 (1980) 608.

16. L. Apker, E. Taft, and J. Dickey, Phys. Rev. 74 (1948) 1462.

17. S. A. Chambers and L. W. Swanson, Surf. Sci. 131 (1983) 385.

18. R. E. Watson and M. L. Perlman, Surf. Sci. 122 (1982) 371.

TABLE I

Work function and AES summary for the indicated crystal faces and stoichiometries of LaB_6. AES primary beam energy 5 kV. Relative dipole contributions $\Delta\phi_D$ to the work function of various crystal faces are indicated.

Plane	$\Delta\phi_D$(eV) (n = 1)		B(179)/La(625) (T = 300 K)	ϕ_F(300 K) (eV) ± .05	ϕ_e(1600) (eV) ± .04
$LaB_{6.09}$(310)	--		4.8	2.50	2.42
$LaB_{6.09}$(210)	-11.38*	-6.48	4.1	2.55	2.46
$LaB_{6.09}$(100)	-10.94		4.4	2.69	2.57
$LaB_{5.86}$(100)	-10.94		4.6	2.60	2.52
$LaB_{5.86}$(110)	-6.05*	0.00	5.8	2.65	2.64
$LaB_{5.86}$(111)	0.00*	+7.34	6.1	2.90	2.90
$LaB_{6.09}$(211)	--		5.1	3.05	2.92

*Based on reconstructed surfaces

TABLE II

Auger peak height ratios for in situ fractured and annealed LaB_6(100) crystals. Primary beam energy 5.0 kV and T = 300 K.

	$\frac{B(179)}{La(78)}$	$\frac{B(179)}{La(625)}$	$\frac{La(78)}{La(625)}$
Fractured	3.7	5.2	1.4
Annealed (1700 K)	1.0	4.6	4.6

Figure Captions

Figure 1. Plot shows the variation of the FN slope of a LaB_6 emitter (after initial field evaporation in H_2 at 77K) with two minute heating intervals at the indicated temperatures.

Figure 2. Graph of H_2 BIV(kV) versus LaB_6 emitter radii. Emitter radii calculated by FIM ring counting between (100) and (210) planes.

Figure 3. FIM (unprimed) and FEM (primed) patterns. The BIV = 13KV for the hydrogen ion images. The patterns at the indicated temperatures correspond to a point on Figure 1.

Figure 4. Variation of the thermionic work functions ϕ_e with temperature for the (100), (310) and (210) crystal faces.

Figure 5. Sideview of (100), (110), (111), and (210) faces of LaB_6. Dashed circles represent the proposed vertical displacement of La atoms due to surface layer reconstruction.

Figure 6. Crystallographic map of the work function distribution for $300 < T < 1600$ K based on the results of this study.

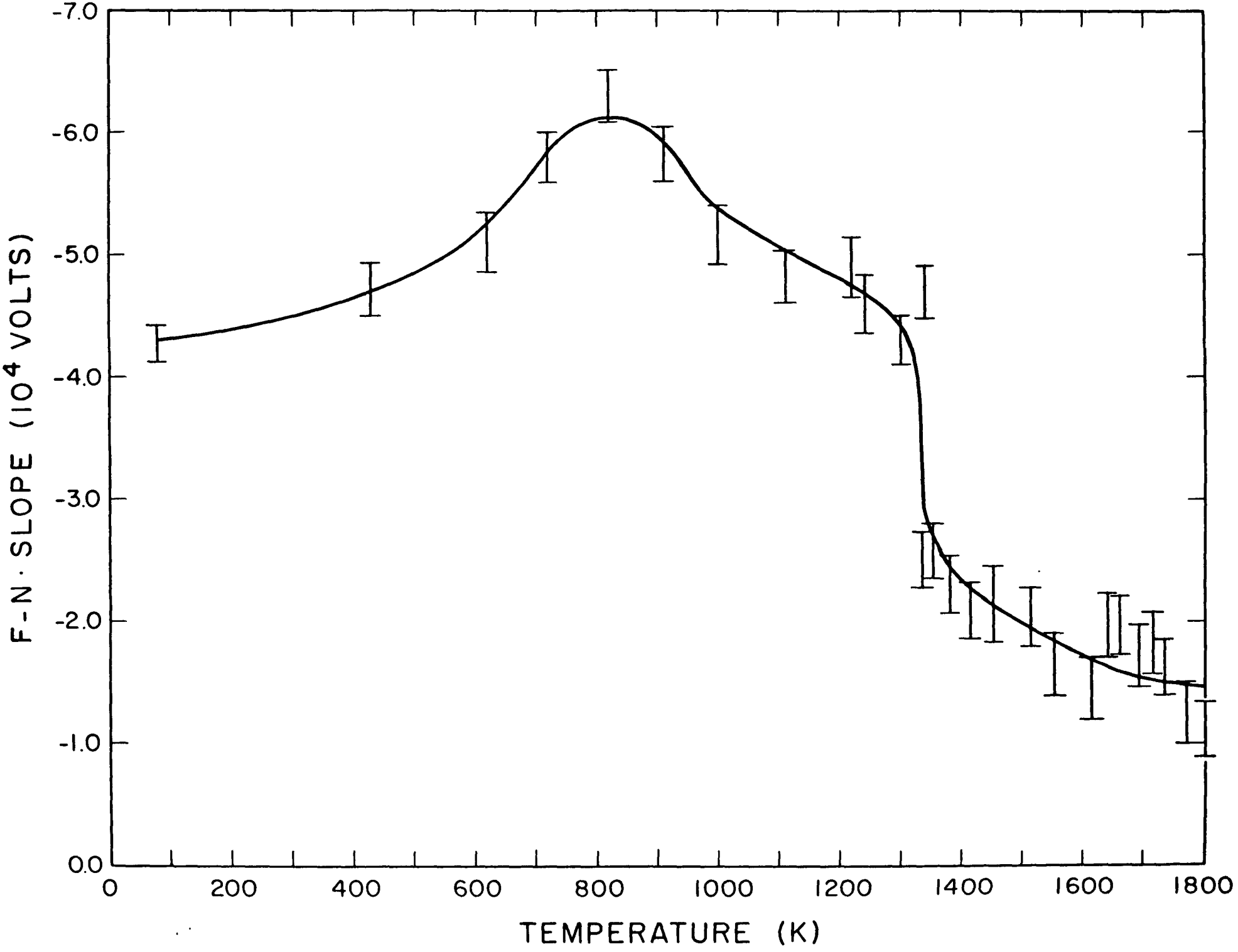
-7.0
-6.0
-5.0
-4.0
-3.0
-2.0
-1.0
0.0
F-N · SLOPE (10^4 VOLTS)
0
200
400
600
800
1000
1200
1400
1600
1800
TEMPERATURE (K)

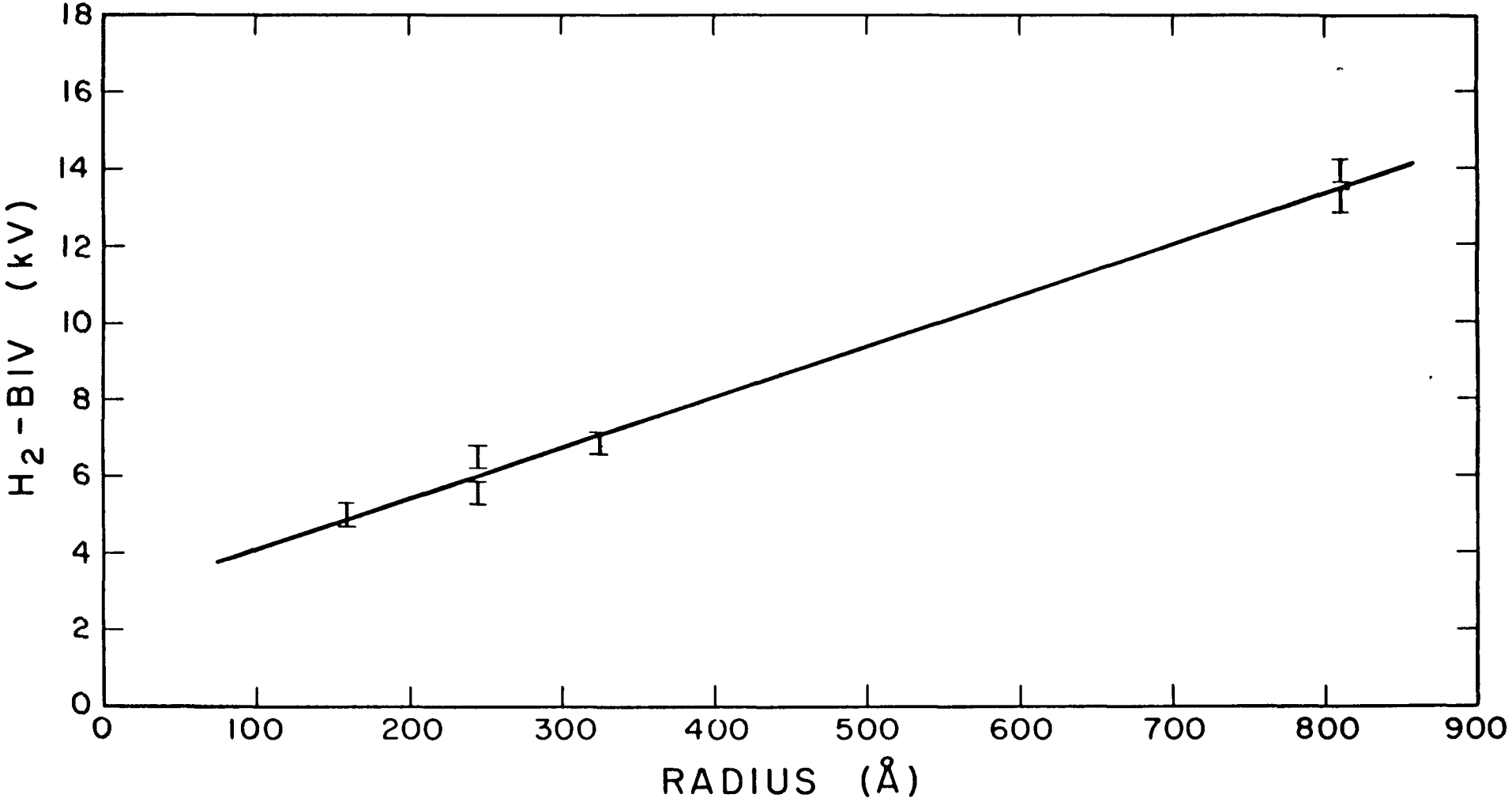
18
16
14
12
10
8
6
4
2
0
H_2-BIV (kV)
0
100
200
300
400
500
600
700
800
900
RADIUS (Å)

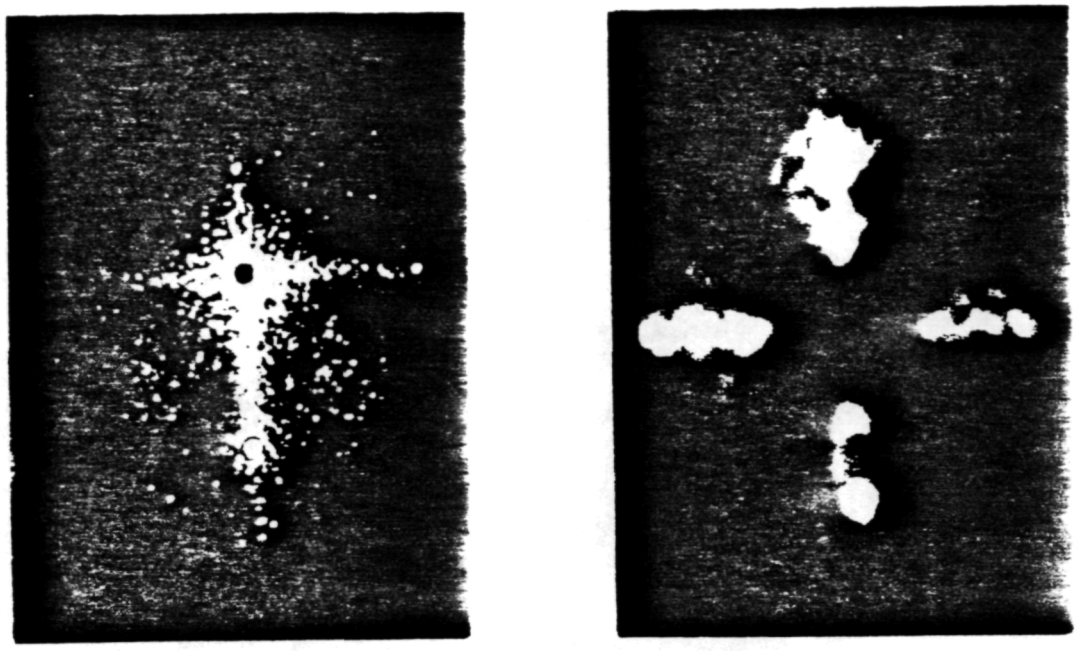

(a) (a')

T = 77 K

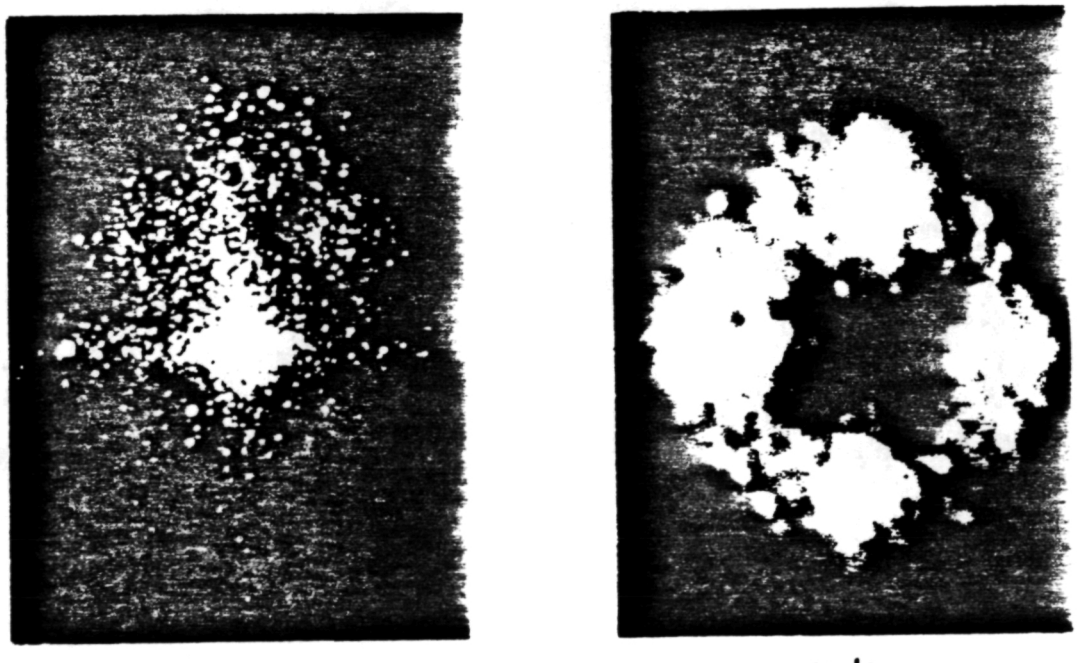

(b) (b')

T = 910 K

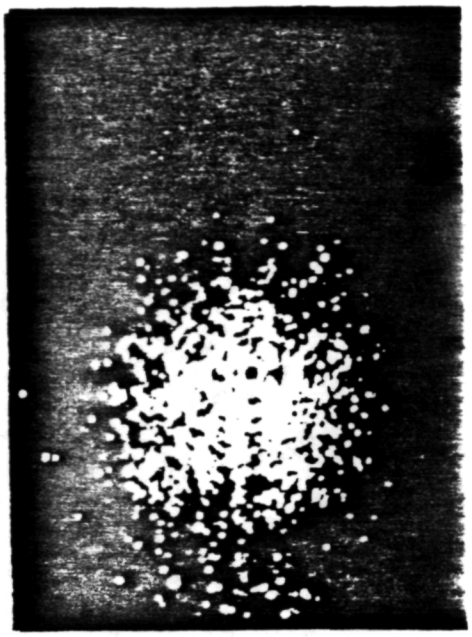

(c)

(c')

T = 1295 K

(d)

(d')

T = 1355 K

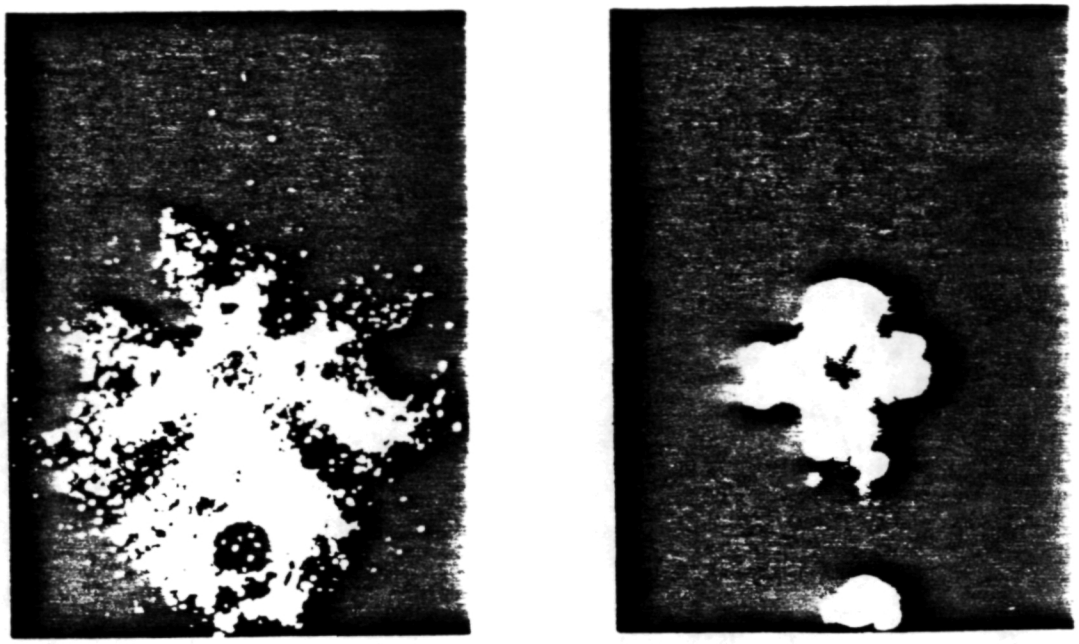

(e) (e')

T = 1410K

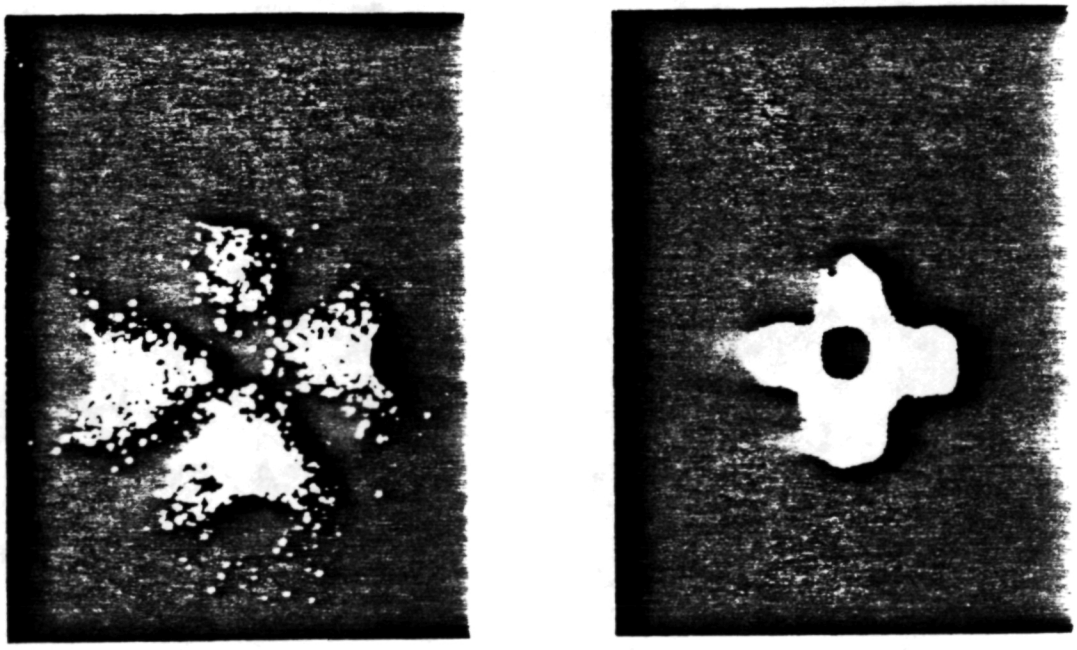

(f) (f')

T = 1770K

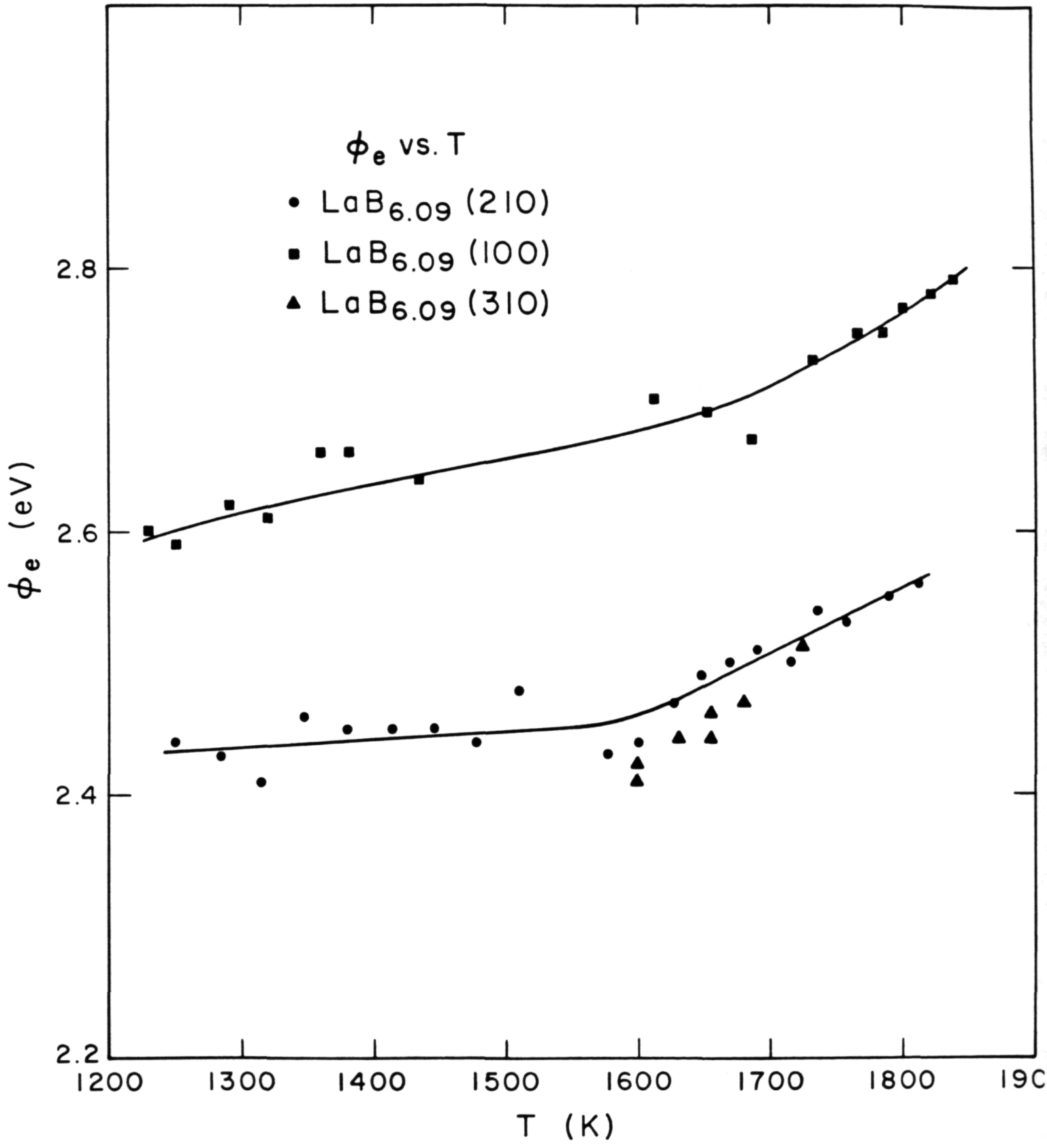
ϕ_e vs. T
• $LaB_{6.09}$ (210)
■ $LaB_{6.09}$ (100)
▲ $LaB_{6.09}$ (310)
ϕ_e (eV)
2.8
2.6
2.4
2.2
1200
1300
1400
1500
1600
1700
1800
T (K)

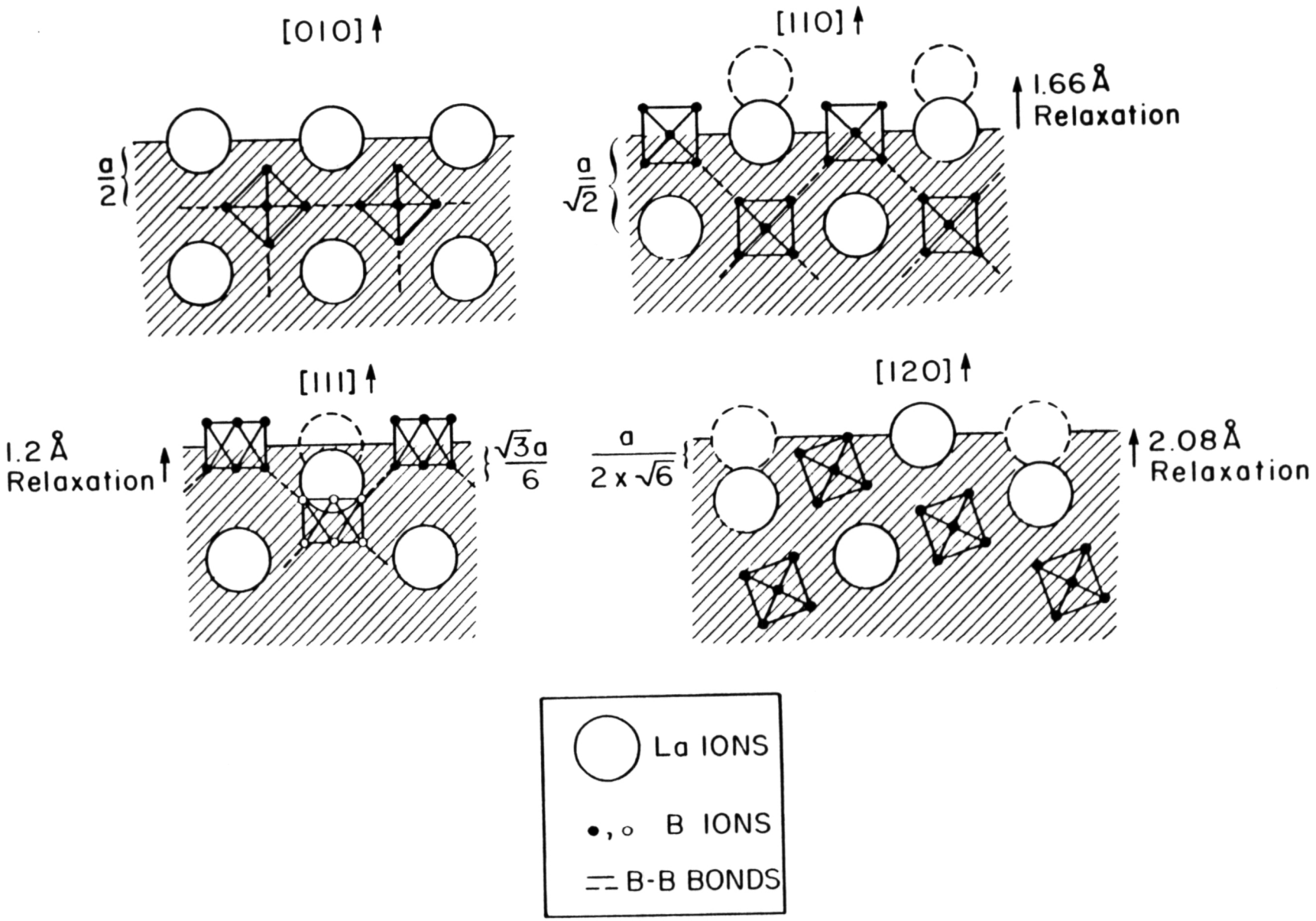
[010]
a/2
[110]
1.66 Å
Relaxation
a/√2
[111]
1.2 Å
Relaxation
√3a/6
[120]
a/2x√6
2.08 Å
Relaxation
La IONS
B IONS
B-B BONDS

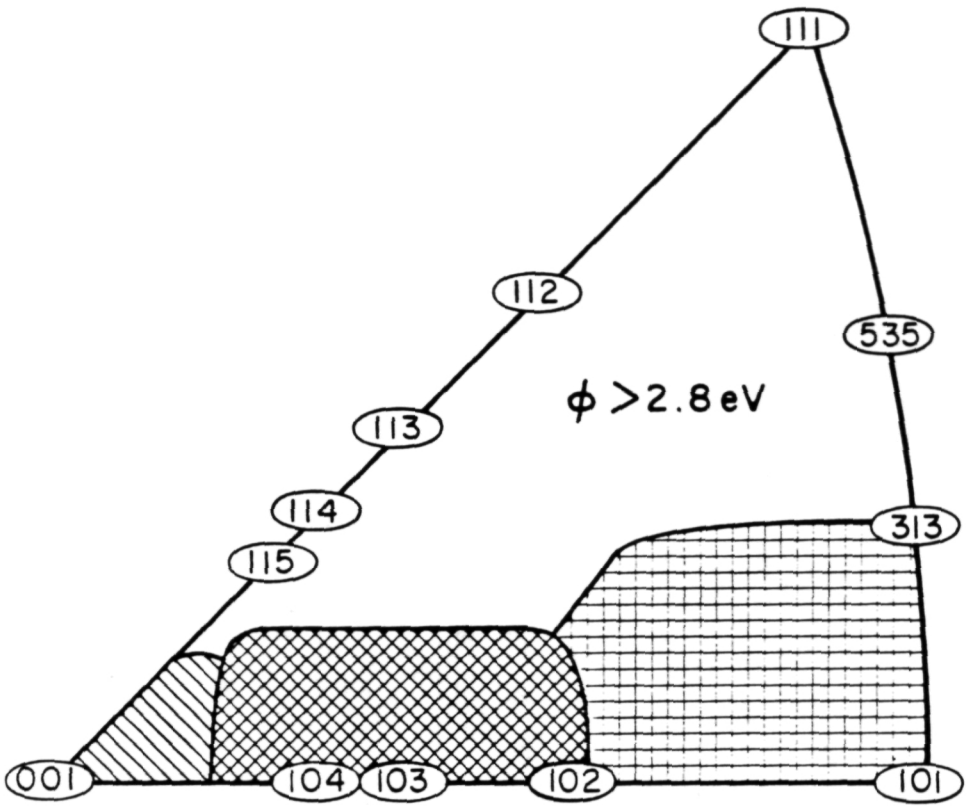

$2.40 < \phi < 2.55$ eV

$2.55 < \phi < 2.65$ eV

$2.65 < \phi < 2.70$ eV